QUANTUM INFORMATION PROCESSING IN NOISY ENVIRONMENTS

By

SREETAMA DAS

PHYS08201305005

Harish-Chandra Research Institute, Prayagraj

A thesis submitted to the

Board of Studies in Physical Sciences

In partial fulfillment of requirements

for the Degree of

DOCTOR OF PHILOSOPHY

of

HOMI BHABHA NATIONAL INSTITUTE

January, 2020

Homi Bhabha National Institute[1]

Recommendations of the Viva Voce Committee

As members of the Viva Voce Committee, we certify that we have read the dissertation prepared by Sreetama Das entitled "Quantum Information Processing In Noisy Environments" and recommend that it may be accepted as fulfilling the thesis requirement for the award of Degree of Doctor of Philosophy.

Chairman – Prof. Pinaki Majumdar		**18-12-2020**
Guide / Convener – Prof. Ujjwal Sen		**18-12-2020**
Examiner - Prof. R. Prabhu		**18-12-2020**
Member 1- Prof. Aditi Sen (De)		**18-12-2020**
Member 2- Prof. Arun Kumar Pati		**18-12-2020**
Member 3- Prof. Sumathi Rao		**18-12-2020**

Final approval and acceptance of this thesis is contingent upon the candidate's submission of the final copies of the thesis to HBNI.

I/We hereby certify that I/we have read this thesis prepared under my/our direction and recommend that it may be accepted as fulfilling the thesis requirement.

Date: 18-12-2020

Place: Prayagraj

Prof. Ujjwal Sen
(Guide)

[1] This page is to be included only for final submission after successful completion of viva voce.

STATEMENT BY AUTHOR

This dissertation has been submitted in partial fulfilment of requirements for an advanced degree at Homi Bhabha National Institute (HBNI) and is deposited in the Library to be made available to borrowers under rules of the HBNI.

Brief quotations from this dissertation are allowable without special permission, provided that accurate acknowledgement of source is made. Requests for permission for extended quotation from or reproduction of this manuscript whole or in part may be granted by the Competent Authority of HBNI when in his or her judgement the proposed use of the material is in the interests of scholarship. In all other instances, however, permission must be obtained from the author.

Sreetama Das

DECLARATION

I, hereby declare that the investigation presented in the thesis has been carried out by me. The work is original and has not been submitted earlier as a whole or in part for a degree / diploma at this or any other Institution / University.

Sreetama Das

List of publications arising from the thesis

Journal:

1. "Inhibition of spreading in quantum random walk due to quenched Poisson-distributed disorder", Sreetama Das, Shiladitya Mal, Aditi Sen De, Ujjwal Sen, *Phys. Rev. A*, **2019,** *99,* 042329.

2. "Necessarily transient quantum refrigerators", Sreetama Das, Avijit Misra, Amit Kumar Pal, Aditi Sen De, Ujjwal Sen, *Europhys. Lett.*, **2019**, *125*, 20007.

3. "Adiabatic freezing of entanglement with insertion of defects in a one-dimensional Hubbard model", Sreetama Das, Sudipto Singha Roy, Himadri Shekhar Dhar, Debraj Rakshit, Aditi Sen De, Ujjwal Sen, *Phys. Rev. B*, **2018**, *98*, 125125.

Preprint:

1. "Almost Markovian Maps and entanglement-based bound on corresponding non-Markovianity", Sreetama Das, Sudipto Singha Roy, Samyadeb Bhattacharya, Ujjwal Sen, arXiv:1906.06198.

Sreetama Das

DEDICATIONS

Dedicated to my parents

ACKNOWLEDGEMENTS

First and foremost, I would like to convey my gratitude and respect to my supervisor Prof. Ujjwal Sen, for his sincere mentoring, unlimited patience, continuous encouragement, and kind words. His friendly and helpful nature, in and out of academia, surely made the 4 years of the PhD journey much easier.

I also sincerely thank Prof. Arun Pati and Prof. Aditi Sen De, as I have learnt many things from them through academic collaborations and discussions. I am grateful to my collaborators Avijit Misra, Amit Kumar pal, Titas Chanda, Chiranjib Mukhopadhyay, Samyadeb Bhattacharya, Sudipto Singha Roy, Himadri Shekhar Dhar, Debraj Rakshit, Shiladitya Mal, Jayanth Jayakumar, Indranil Chakraborty, Chirag Srivastava, Ahana Ghoshal, Kornikar Sen, from whom I have been enriched a lot. Cheers to the whole QIC group, for always being with each other, from arranging wonderful conferences to cooking, playing, and travelling together. I am extremely fortunate that as I was taught at HRI by a bunch of wonderful and benevolent teachers, to whom I convey my deepest gratitude. Their presence made all the HRI events more enjoyable.

My wholehearted love and good wishes goes to my friends at HRI- Sumana, Deepika, Juhi, Shouvik, Gautam, Dhruv, Sarif, Ratul, Tanaya, Alam, Sohail, Sushovan, Sumon, Atri, Sankha, Stav, Bidisha, Jaitra, Subha. Thanks to Nirnoy, Titas, and Dipyaman, for suggesting good movies. Cheers to the “Bawal” and “SteepingTea" group- Saptarshi, Dipyaman, Souvik, Suparna, Anindita, Rudra and Kathakali. Thanks to Dipyaman and Chiranjib, it was lovely to have known you for such long time.

I thank all the teachers in my school for their lifelong teaching, kindness and love. Thanks to Sohini and Shreyasi, for always being with me.

Finally, I express my respect and love towards my family, for always supporting and encouraging me to chase my dreams, and bearing with me at those times when I failed to give them my time.

Contents

List of Figures

List of Tables

7

Conclusions

In this thesis, we looked into a number of effects that an environment, and environment-induced noise, can have on an open quantum system. The study is mainly based around the aspects like- quantification of non-Markovianity, transient cooling in a quantum refrigerator, entanglement freezing in t-J model, and inhibition of spreading in quantum random walk. The topics are comprised of both where it is possible to explicitly model the system-environment interaction, and also the cases when the presence of the environment can be described by an effective Hamiltonian of the system.

After two introductory chapters, we began in the third chapter with a conceptualization of a set of dynamical maps, termed as "ϵ-Markovian" maps corresponding to the open system, such that when those maps are extended to a higher-dimensional Hilbert space corresponding to system and environment, the time-evolved joint state, at all time, has a mutual information less than a fixed quantity ϵ. We then quantified the "$\epsilon-$nonmarkovianity" of a dynamical map, by considering the minimized distance of that map from the set of "ϵ-Markovian" maps. We have analytically derived a bound on the non-Markovianity measure, which depends on an entanglement-like quantity between the system and its immediate environment. If either of the non-Markovianity and entanglement is known, it is possible to estimate the other from this bound.

As a practical realization of an open quantum dynamics, in the next chapter, we con-

sidered a three-qubit quantum absorption refrigerator. There were three thermal baths at different temperatures, each of them acted as the environment of one qubit. The baths were for supplying free energy for the functioning of the refrigerator. The inter-qubit interaction, as well as the qubit-bath interaction led to a cooling of one of the qubits. We pointed out that, there are some regions in the qubit-bath interaction parameter space, where the steady state cooling is absent or negligible, but there exists significant amount of transient cooling. A particular form of the interaction parameters, which we called "canonical interaction parameters (CIP)", were useful to describe the phenomenon. With a modification in the CIP, we obtained another interesting picture, where the qubit monotonically cools down to the steady state temperature in a very short time. The results were obtained by modeling the qubit-bath interaction parameter in two different ways.

We then considered the t-J model, which is an example of a quantum many-body system in presence of doping. We numerically obtained the ground state of the corresponding Hamiltonian by using the Lanczos algorithm. We calculated the bipartite and multipartite entanglements in the ground state. We observed that the bipartite entanglement remains frozen in the metallic phase of the model, with respect to adiabatic changes in the system parameters. In contrast, the multipartite entanglement is frozen for system parameters exceeding the boundary of metallic region, but only in the low electron density regime. As entanglement is a very useful resource in quantum information processing, a frozen value of entanglement can provide a significant advantage in quantum information protocols.

Finally, we studied the effect of disorder on a one-dimensional quantum random walk. In an ordered quantum walk, after each coin toss (or equivalently, at each time step), the particle can jump one step left / right depending on the outcome of the coin. We introduced a quenched disorder in the jump-length, i.e., after each coin toss, the number of steps to be taken, is randomly chosen from some integer probability distribution. By varying the number of steps, we obtained a scaling behaviour of the standard deviation of the probability distribution of the walker's position, which showed that the speed of

the particle reduces in comparison to the ordered quantum walk. In an ordered quantum walk the standard deviation is proportional to T, the number of steps. Whereas, in the quenched disordered case, the standard deviation varies as approximately $T^{0.8}$, for a variety of integer probability distributions, which clearly demonstrates that the disorder can cause an inhibition in spreading of the random quantum walker.

The presence of environmental noise can be detrimental as well as useful in various aspects of quantum information processing. On one hand, a disorder in jump length can cause a reduced speed of a quantum walker, resulting in slowdown of quantum search algorithms, which heavily depend on quantum random walks. On the other hand, the presence of disorder in the form of doping in systems described by t-J model, can provide a robust bipartite and multipartite entanglement, which is indeed very crucial for large number of quantum information protocols. Along with identifying such positive as well as detrimental effects of noise in quantum devices, we also look at devices that inherently interact with an environment. A general picture of such system and its characterization with respect to Markovianity was taken up in Chapter 3, while a system of three qubits, immersed in thermal baths as their environments, was shown to act as a small necessarily-transient quantum refrigerator.

SUMMARY

In this thesis, we study various effects of an interacting environment on a quantum system. Our study includes the cases when the Hamiltonian of such an open quantum system is ordered, as well as the cases when the environment induces disorder in the Hamiltonian. In Chapter 1, first we give a brief introduction to the dynamics of an ordered open quantum system. We describe the classification and traits of Markovian and non-Markovian evolutions. Then we discuss the effects of the environment-induced disorder on the system.

In Chapter 2, we give a brief account of entanglement and the resource theoretic structure of entanglement. We will also discuss a number of entanglement measures that we have subsequently used in the following chapters of the thesis.

In Chapter 3, we study a class of dynamical maps of an open quantum system, such that the dilation of these maps into higher-dimensional system-environment Hilbert space, always lead to a system-environment state, which has non-zero mutual information. Particularly, the mutual information of these states, for all times, remain less than or equal to ϵ. The corresponding dynamical maps of the system is called "ϵ-Markovian" maps in our work. We propose that, the "ϵ-nonmarkovianity" of a general dynamical map can be quantified by minimizing its distance from the set of ϵ-Markovian maps. We also analytically derive a bound on ϵ-nonmarkovianity, which depends on the entanglement between the system and environmnent.

In Chapter 4, we consider a three-qubit quantum absorption refrigerator, where three interacting qubits are in thermal contact with three different thermal baths. The qubit-bath interaction in such a refrigerator has been modelled by using a simple toy model, as well as by explicitly treating the bath as a collection of harmonic oscillators. It has been shown that both the models, can result in cooling of one of the qubits, both in steady state and transient state of the three-qubit system. We show that, it is possible to achieve significant transient cooling even when there is no/negligible steady state cooling. Specifically, a

particular form of qubit-bath interaction parameter, which we called “canonical interaction parameters"(CIP), facilitates this phenomenon. A particuar alternation to CIP leads to a fast cooling, where the minimum temperature is reached in a very short time, and this temperature is retained in steady state.

In Chapter 5, we deal with the scenario, where the environmental noise is present in the form of doping in a spin chain. Particularly, we consider a one-dimensional t-J model, and study the bipartite and multipartite entanglement in the ground state of this model. We observe that the bipartite entanglement is frozen with respect to adiabatic change in the system parameter J/t, in the metallic phase i.e. when $J/t < 2$. Unlike bipartite entanglement, the multipartite entanglement is frozen across regions beyond $J/t > 2$, but this freezing breaks for higher electron density. However, such freezing of entanglement with respect to changing system parameters has not been observed in absence of doping.

In Chapter 6 we consider a one-dimensional discrete quantum walk, and introduce a type of disorder which has not been explored before in the context of quantum random walk. We consider that, after each coin-toss, instead of taking one step left/right, the particle can jump “j" number of steps left or right. The number “j" is randomly chosen from Poisson distribution, and we calculate the quenched averaged standard deviation of the walker over a large number of configurations of this disorder. The scaling behaviour of this averaged standard deviation with increasing number of steps shows that, the scaling exponent is approximately 0.8, which is less than the scaling exponent 1 in the case of ordered quantum walk. This proves that, the disorder gives rise to an inhibition of spreading of random walker. Moreover, the scaling exponent remains same when “j" is chosen from certain sub- and super- Poissonian distributions. We conclude the thesis in Chapter 7.

1 Introduction

1.1 Time evolution in closed ordered quantum system

While talking about the quantum mechanical behavior of a system, the simplest picture is to consider that the system is not interacting with any other auxiliary system, i.e. the system is “closed" (in the sense of being isolated). Here, the auxiliary system can be any another quantum mechanical system having a number of degrees of freedom which is independent of that of the main system, and serves the purpose of being the system’s “environment". When a quantum system is perfectly isolated from any other auxiliary system, so that the environment is “inert", the time evolution of the system is effected by a unitary operator, and mathematically described by the Schrodinger’s equation, which can be written in the following form:

$$\frac{\partial|\Psi(t)\rangle}{\partial t} = -\frac{i}{\hbar}H|\Psi(t)\rangle, \tag{1.1}$$

where $|\Psi(t)\rangle$ is the pure state wave function describing the system, and H is the Hamiltonian of the system. In case the system is in a mixed state $\rho(t)$, the above equation takes the general form,

$$\frac{\partial\rho(t)}{\partial t} = -\frac{i}{\hbar}[H,\rho(t)]. \tag{1.2}$$

The quantum mechanical observables of the system, which commute with the Hamiltonian of the system, remain conserved in such a time evolution. Examples of observables and their functions that may remain conserved are energy, momentum, etc. Due to the absence of interaction with any other system, there is no noise or damping present in the system and so the system dynamics is devoid of any form of decay or decoherence. If additionally, the system Hamiltonian is free from any disorder in its parameters, the disorder-induced effects are also absent. However, this is a highly idealistic picture, and in a real situation, it is hardly possible to perfectly isolate a system from any kind of interaction with auxiliary systems and remove all disorders.

1.2 Time evolution in ordered open quantum system

The field of open quantum systems deals with the general scenario when our system of consideration, S, is "open", i.e. it is interacting with other systems or its environment E. Due to this interaction, there is inevitably some "loss" of information about system properties, which manifests itself in the form of dissipation of energy, decay of coherence, etc. in the system state. When more than one system are interacting among themselves, then looking at one particular system, its time evolution is almost never unitary, and can almost never be mathematically represented in the form of a Schrodinger's equation. The evolution of the total system (if not interacting with any other system), is, within quantum theory, of course a unitary time evolution. So, if $\rho_{SE}(0)$ is the initial joint state of system and environment, then the time-evolved joint state is $\rho_{SE}(t) = U(t)\rho_{SE}(0)U(t)^\dagger$, where $U(t)$ is the corresponding unitary time-evolution operator on the system-environment joint Hilbert space $\mathcal{H}_S \otimes \mathcal{H}_E$. Now the reduced state of the system at time t is obtained by tracing out the environmental degrees of freedom, i.e.,

$$\rho_S(t) \equiv \Lambda_S(\rho_S(0)) = \mathrm{Tr}_E(\rho_{SE}(t)), \tag{1.3}$$

where $\rho_S(0)$ is the initial state of S. Here,

$$\Lambda_S(\rho_S(0)) = \mathrm{Tr}_E(U^\dagger(t)\rho_{SE}(0)U(t)) \tag{1.4}$$

is the generally non-unitary time evolution operator of the reduced system S, and is usually referred to as *"dynamical map"*. The corresponding time differential equation of the evolution of S can be generally referred to as the *"master equation"*. Now, if the initial state of the total system is $\rho_{SE}(0) = \rho_S(0) \otimes \rho_E(0)$, then one finds from Eq. (1.3), that the evolution can be written as

$$\rho_S(t) = \sum_i K_i \rho_S(0) K_i^\dagger, \tag{1.5}$$

where the *Kraus operators* K_i's are functions of the time difference, t, between the initial and final times, the initial state of the environment, and the unitary U_{SE}. The Kraus operators satisfy the relation $\sum_i K_i^\dagger K_i = \mathbb{I}$, where $\mathbb{I}$ is the identity operator on the system Hilbert space. In this case, the dynamical maps are *completely positive trace preserving* (CPTP) operations and they form a *dynamical semigroup*. The time-reversal operation is not possible within such a dynamics. Also, if the state $\rho_{SE}(0)$ is not a product state, then the dynamical map that takes $\rho_{SE}(0)$ to any other $\rho_{SE}(t)$, may not be a CPTP map for all time t.

From Eq. (1.3), it is easy to see that, due to the possible build-up of correlation between the system and environment, the state of S at some time $t \neq 0$, depends not only on the system state $\rho_S(t_1)$ at some earlier time $t_1 < t$, but also on the environment state $\rho_E(t_1)$ at time t_1. This implies that the environment retains some information about the system; or in other words, there is an "information flow" from the system to the environment. There can also be a temporal backflow of information from the environment to the system. To construct $\rho_S(t)$, one should have a prior knowledge about the system state at all earlier times $t_2 < t$, i.e. the reduced dynamics is not time-local. But, if the number of degrees of freedom of the environment is very large, it becomes difficult to mathematically calculate the reduced dynamics of the system. However, considerable

simplifications can be obtained by assuming a number of conditions on the nature of the environment and the coupling between system and environment. In most physical situations, these assumptions are not practical, but they can be a good approximation in some particular limits, as will be discussed in the following section.

1.2.1 An overview of Markovian dynamics

In this section, we will present a brief idea of Markovian dynamics. Examples of such dynamics will be discussed in Chapter 3 and Chapter 4. The bunch of assumptions, used to simplify the reduced dynamics in this case, is called *Born-Markov approximations*. Together, they give rise to the Markovian dynamics of the open quantum system. These approximations work well in the weak-coupling limit, i.e., when the coupling between the system and environment is weak. In this limit, one can coarse-grain the time scales corresponding to the system and environment degrees of freedom, and assume that they obey a certain condition between them, namely- the evolution time-scale of the system t_S is much larger than the correlation time scale of the environment t_E. This results in the physical picture where environmental mode excitations decay in a time which is much shorter than the system evolution time, implying that for every time slot in which the system has changed appreciably, the environment effectively forgets all the information acquired from the system. This lost information can never creep back to the system, and hence the dynamics is also called *memoryless interaction*. This also removes the dependency of the state $\rho_S(t + dt)$ on the initial state $\rho_S(0)$, but only on the instantaneous state $\rho_S(t)$. Thus, the Markovian dynamics is characterized by a one-way information flow from system to the environment.

In the weak coupling limit, owing to the above assumption, one can have the following mathematical simplifications:

$C1$. At any time t, we can write the total state $\rho_{SE}(t)$, as a product state of system and

environment in the following way

$$\rho_{SE}(t) \approx \rho_S(t) \otimes \rho_E(0), \tag{1.6}$$

where $\rho_S(t) = \mathrm{Tr}_E(\rho_{SE}(t))$. It means that the system has evolved, but as the environment correlation time is very small, the environment effectively remains in the same state as the initial state $\rho_E(0)$. This assumption is called *Born approximation*.

$C2$. The state $\rho_S(t+dt)$, after infinitesimal time dt from t, depends only on the immediate state $\rho_S(t)$ at any time t, and does not depend on states at earlier times. This is called *Markov approximation*.

$C3$. And finally, one neglects all the high-frequency components in the Hamiltonian, and this is called the *rotating wave* approximation.

If assumption $C1$ holds true for a time interval $0 \leq t \leq T$, then between any two times t_0 and t_2, the dynamical map $\Lambda_S(t_2, t_0)$ can be written as

$$\Lambda_S(t_2, t_0) = \Lambda_S(t_2, t_1)\Lambda_S(t_1, t_0). \tag{1.7}$$

If the above assumptions hold true, then the dynamical map Λ_S is called *divisible* in the interval $0 \leq t \leq T$. In Eq. (1.7), it is possible to decompose the right hand side in more than two terms in the following way, e.g.,

$$\Lambda_S(t_n, t_0) = \Lambda_S(t_n, t_{n-1})\Lambda_S(t_{n-1}, t_{n-2})....\Lambda_S(t_1, t_0). \tag{1.8}$$

where, $t_0 < t_1 < ... < t_{n-2} < t_{n-1} < t_n$. Eq. (1.8) is the quantum analogue of the classical *Chapman-Kolmogorov* equation, which holds true if a classical stochastic process is Markovian. Similar to the classical case, if a quantum dynamical map is divisible, then the corresponding dynamics may be referred to as Markovian.

With the above assumptions, it is possible to write a master equation corresponding to

"Markovian" dynamics of the reduced system. This master equation, which is called the *Lindblad master equation*, has the following form:

$$\frac{d\rho_S}{dt} = -i[H_0, \rho_S(t)] + \sum_{i,j} \gamma_{ij}\Big(L_j \rho_S(t) L_i^\dagger - \frac{1}{2}\{L_i^\dagger L_j, \rho_S(t)\}\Big). \tag{1.9}$$

Here, H_0 is the effective Hamiltonian of the system that is responsible for the unitary part of the evolution, $\gamma_{ij}(\omega)$ are the decay rates, and L_i's are the Lindblad operators which corresponds to the jump between those eigenstates of the total Hamiltonian, which has an energy difference ω_i. It is possible to generalize Eq. (1.9) to the case of time-dependent H_0 and γ_{ij}. The dynamical map corresponding to Eq. (1.9) can still satisfy the divisibility property. Such a master equation is "Markovian", if $\gamma_{ij}(t) \geq 0$, for all time t and for all i, j. We will specifically solve a master equation of the form Eq. (1.9) in Chap. 4 for both steady and transient states. For a detailed microscopic derivation of the master equation, see [1].

A system undergoing Markovian dynamics, always monotonically approaches a steady state. This monotonic approach to steady state is associated with the monotonic decay of other system properties like- entanglement with an auxiliary system, coherence of the system, etc. Due to this decaying nature, Markovian processes are detrimental for quantum information and communication tasks, which requires to preserve the correlation and coherence of the system against environmental perturbation. However, the deviation of a quantum dynamics from Markovianity, is a more realistic case, and also can prove to be advantageous for quantum informatic protocols, as we will discuss in the following section.

1.2.2 Deviation from Markovianity: non-Markovian dynamics

In most of the realizable physical scenarios, the dynamics is not Markovian. The system and environment build up correlation between them in the course of time evolution, and

then the CP-divisibility of the dynamics breaks down. Physically, this means that there is two-way information flow between the system and environment, i.e. the environment remembers the system. The master equation corresponding to a non-markovian dynamics, may or may not be expressible in Lindblad form. A time-local master equation of the form Eq. (1.9) describes non-Markovian dynamics, if at least one of the decay rates $\gamma_{ij}(t)$ is negative for some interval of time. It is evident that the corresponding dynamical map will not be CP-divisible. In Chap. 3, we will consider such time-local master equations which, depending on the decay rates, can give rise to both Markovian and non-Markovian dynamics. Unlike the Markovian case, in non-Markovian dynamics, due to the environment-to-system information backflow, the decay of the system properties can be non-monotonic, i.e. there may exist some temporal regain / revival, which may then be useful for quantum information processing tasks.

In the past years, a large number of non-Markovianity measures and witnesses have been proposed. We will briefly discuss about them in the next chapter. As discussed in the last paragraph, non-markovianity may act as a resource in a number of quantum information processing tasks. It was shown that in quantum teleportation, even if the shared entangled state is subject to decoherence, the information backflow effects can be used to perfectly execute quantum teleportation with mixed states [2]. Non-Markovian channels can lead to a higher efficiency of quantum channels, compared to the Markovian ones [3]. It has been experimentally demonstrated that nonlocal memory effects also help in distribution of polarization entangled pair of photons in optical fibres and in extracting work from Otto cycles [4]. A resource-theoretic structure of non-Markovianity has been put forward in [5]. In spite of this progress, a clear definition of non-Markovianity is still under study. In Chap. 3, we propose a new measure of non-Markovianity, which is independent of the previous ones and we are able to analytically derive a bound on this non-Markovianity in terms of entanglement between system and environment.

1.3 Effect of interaction with noisy environment

A closed system governed by an ordered Hamiltonian is, in a large majority of situations, an idealization. Previously, we have discussed about open quantum systems, in which the system and environment are still governed by an ordered Hamiltonian. In this section, we consider a different practicality, viz an effectively closed system governed by a disordered Hamiltonian. The disorder or inhomogeneity is of course caused by an environment. But, we work in the limit in which the effect of disorders and inhomogeneities is encapsulated within an effective disordered Hamiltonian of the system only, without referring directly to the environment.

The disorder can be present naturally in the system, or can be artificially introduced, e.g. by doping of solid state materials with holes. We are considering the situation where the exact interaction Hamiltonian between the system and environment, which causes the disorder, is either unknown or too complicated to handle; but we can write an effective Hamiltonian of the system which takes into account the presence of the disorder. By solving this effective Hamiltonian, one can get many useful insights about some particular physical entity of the system. An outstanding example is *Anderson's localization*, first noted by P. W. Anderson in 1958. The work demonstrates that, if there is some randomness present in the lattice potential, the wave-packet of the electrons can become localized. In many-body systems, the presence of holes in the lattice can be considered to be incorporated due to a noisy environment. This inhomogeneity can result in fascinating characteristics of quantum mechanical properties of the system, which are absent in the otherwise ordered system. Entanglement is a well-known quantum mechanical attribute, which plays a key role in many quantum information and communication protocols, e.g. quantum teleportation, entanglement-based quantum key distribution, etc. In the succeeding chapter, we will discuss the resource theory of entanglement and various entanglement measures used in this thesis. As many-body systems are useful substrates in many such protocols, it is important to know how entanglement behaves in many-body

systems, in presence of environmental noise. Motivated by this, in Chap. 5, we study the entanglement behaviour in the ground state of a "t-J" model, and surprisingly observe a freezing of entanglement with respect to system parameters.

Besides the above scenario, due to presence of disorder, one or more parameters in the system Hamiltonian may assume random values. For a particular value of the randomness, the system dynamics can be written in the form of Eq. (1.2). But in order to obtain an idea about the physically relevant behavior of a particular property of the system in presence of such randomness, we need to do an averaging of that property over a large number of random realizations of the parameters. The averaging strategy depends on the relative value of system timescale τ_S and disorder timescale τ_D, where, τ_S is the time during which we observe the system properties and τ_D is the time it takes for the disorder to equilibrate in the system. We consider the case where the system is "glassy", i.e., $\tau_S \ll \tau_D$, so that for each configuration of the disorder, we calculate the value of the particular property we want to study, and then we perform an averaging of that value over a large number of random configurations of the disorder. Such an averaging is referred to as quenched averaging, and the corresponding disorder as quenched disorder.

In Chap. 6, we apply the quenched avaraging to calculate the average standard deviation of a one-dimensional quantum walker, when there is a randomness in the number of steps the particle can take after each coin toss. There is an extensive literature discussing the effects of randomness present in the lattice of the quantum walk, or randomness present in the coin-operation. It has been observed that such randomness can give rise to a reduced spread of the quantum walker. However, the disorder introduced in our work, has not been studied before. We indeed see that, due to the disorder, the ballistic motion of the particle is hindered. The scaling behaviour of the quenched averaged standard deviation with respect to the number of steps, also reveals that the particle's spread is less than that in an ordered quantum walk.

1.4 Thesis overview

The thesis is organised in the following way. In chapter 2, we will briefly discuss about the resource theory of entanglement and different entanglement measures that we have used in this thesis. In chapter 3, we will first look into some already existing non-Markovianity measures. Then we will introduce a new quantifier of non-Markovianity which is independent of the already existing measures. We will derive an inequality, which gives an entanglement-based bound on our measure of non-Markovianity. In chapter 4, we describe the function of a three-qubit refrigerator, where each qubit is interacting with its environment, which is a thermal bath in this case. We begib by considering a simple toy model of qubit-bath thermalization and demonstrate how we obtained a parameter regime where there is a significant transient cooling of the cold qubit, but the steady state cooling is negligible. Next, we studied a more realistic scenario, where the qubit-bath interaction is modeled as memoryless Markovian interaction, and we show that, for the same parameter regime, the same behaviour of the cold qubit temperature is obtained for this thermalization model as well. In chapter 5, we study the Hubbard model, where the environmental noise is present in the form of doping (holes), and we observe a freezing of bipartite and multipartite entanglement in the ground state of this doped model with respect to change in system parameters. Finally, chapter 6 discusses the inhibition of spread in quantum random walk, where there is a disorder in the number of steps the particle can take after each coin toss. We the conclude in chapter 7 with the inferences of the thesis.

2

Entanglement measures

The nature of correlations present between two or more quantum systems can be both classical and quantum. If a bipartite state ρ_{AB} can be written as [6]

$$\rho_{AB} = \sum_i p_i \rho_A \otimes \rho_B, \qquad \sum_i p_i = 1, \tag{2.1}$$

then the correlation present between the two parties, A and B, can be created by local operations and classical communication (LOCC). All states that can be written in the form of Eq. (2.1) are called *separable states*. States that cannot be thus expressed are referred to as "entangled" [7, 8]. These states are fundamentally different from separable ones, and can be used in a plethora of applications.

Entanglement is a purely quantum phenomenon. Entangled states are useful in a large number of quantum information protocols; in this sense, entanglement is an important resource in quantum information processing. There are certain tasks that can be achieved by using an entangled state but is not possible classically. For example, the teleportation of a quantum state between two distant parties is possible when the two parties share certain entangled states between them and they are allowed to classically communicate with each other [9]. Other quantum processes where entanglement acts as a resource are entanglement-based quantum cryptography [10] and quantum dense coding [11].

Entanglement cannot be created between two unentangled and spatially separated par-

ties by doing only local quantum operations on them, even if the parties have access to a classical channel. They must be brought to interact with each other in order to be entangled (a subtle alteration of this definition is needed due to the existence of the phenomenon of entanglement swapping [12, 13]). Suppose, A and B share a joint quantum state ρ_{AB} which is unentangled. Now, A locally performs a set of complete quantum operations A_i on its Hilbert space $\mathcal{H}_A$, such that $\sum_i A_i^\dagger A_i = \mathcal{I}_A$, and classically communicates the outcome "i" to B. Depending on this outcome, B chooses to locally perform an operation B_{ij} on $\mathcal{H}_B$, which belongs to another set of complete quantum operations such that $\sum_j B_{ij}^\dagger B_{ij} = \mathcal{I}_B$, and communicates the outcome "j" to Alice. The whole protocol can then again be repeated. Such a series of local operations and classically communicating the outcome, is called LOCC. LOCCs cannot create entangled state from a separable one. An entanglement measure is usually required to be non-increasing, on average, under LOCC.

This chapter is organized as follows. In section 2.1, we introduce a few entanglement detection criterions, followed by a brief discussion on the resource theory of entanglement in section 2.2, and in section 2.3 we will give an overview of the bipartite and multipartite entanglement measures that we have used in this thesis.

2.1 Entanglement detection criterions

Entanglement in a state can be detected by particular detection criterions. In this section, we will give a brief idea about two such criterions, which will be useful to construct the measures discussed in section 2.3.

1. Positive Partial Transpose (PPT) criterion: If a state is separable, then the partial transposed matrix of that state will always have non-negative eigenvalues [14]. Let $\rho_{AB}^{T_A}$ be the partially transposed matrix of ρ_{AB}, obtained by taking transposition with respect to subsystem A. If $\rho_{AB}^{T_A}$ has at least one negative eigenvalue, we can conclude that ρ_{AB} is an entangled state. Taking partial transposition with respect to the other

subsystem B does not change this property. The converse of this condition is not always true, i.e., there exist states which are entangled, but the corresponding partial transposed matrix has non-negative eigenvalues. These states are called PPT (Positive partial Transpose)-entangled states. However, in $C^2 \otimes C^2$ and $C^2 \otimes C^3$ systems, the PPT criterion is both necessary and sufficient for detecting entanglement [15].

2. Entanglement witness operators: A linear entanglement witness operator $\mathcal{W}$ is a Hermitian operator such that, for certain entangled states ρ, $\mathrm{Tr}(\mathcal{W}\rho) < 0$ and for all separable states σ, $\mathrm{Tr}(\mathcal{W}\sigma) \geq 0$ [15–20]. For every entangled state, there exists a witness operator. Adding non-linear terms to a witness operator can increase its efficiency in the sense that, it can detect entanglement of states additional to those possible with the linear one. So, given a state ρ, if we are able to find an operator $\mathcal{W}$, such that $\mathrm{Tr}(\mathcal{W}\rho) < 0$ and additionally, $\mathrm{Tr}(\mathcal{W}\sigma) \geq 0$, for all separable σ, then we can conclude that ρ is entangled.

   Example: Suppose, ρ is an entangled state with non-positive partial transpose (NPPT). If $|\phi\rangle$ is an eigenvector corresponding to a negative eigenvalue of ρ^{T_A}, then $\mathcal{W} = |\phi\rangle\langle\phi|^T$ is an entanglement witness operator for ρ.

2.2 Resource Theory of Entanglement

Entanglement is clearly a resource in several quantum protocols, including teleportation and dense-coding. Such tasks are impossible to be performed without shared entanglement. This naturally led to a resource theory of entanglement.

Any resource theory has three basic elements- the free states which do not contain the resource, the free operations which cannot increase the amount of resource in a given state, and the resource measures. These three elements, in the context of entanglement theory are as follows.

- Free states: In the resource theory of entanglement, a free state is one which has no entanglement. Clearly, in case of bipartite systems, the separable states written in the form Eq. (2.1) are free states. Separable states form a convex set.

- Free operations: Remaining within the distant laboratories paradigm, using which the set of separable states is defined, the LOCC class forms an interesting class of operations that can be identified as the “free operations", as they can be relatively easy to implement in practice. The general class of operations that cannot create nonseparable states is more complex, and includes separable superoperators [21]. One may also define free operations by requiring non-increase of a certain set of entanglement measures, but this first of all requires a way to identify such a set, and secondly, it can be a difficult task even after the identification is somehow made.

- Entanglement measures: A valid entanglement measure $E(\rho)$ should satisfy certain properties. This set of properties is not a unique one, and is often chosen by looking at the application at hand, or the motivation that one wishes to be swayed by. See e.g. [22]. An exemplary set of axioms is given in the following list.

  i) **Faithfulness:** $E(\rho) \geq 0$, and the equality holds iff $\rho \in \mathcal{S}_{AB}$, where $\mathcal{S}_{AB}$ is the set of free states.

  ii) **Monotonicity:** the entanglement of a state should not increase under the action of LOCCs, so that $E(\rho) \geq E(\Lambda(\rho))$, where Λ is an LOCC map.

  iii) **Invariance under local unitary operations:** $E(U_A \otimes U_B \rho_{AB} U_A^\dagger \otimes U_B^\dagger) = E(\rho_{AB})$.

  iv) **Convexity:** the entanglement doesn’t increase under mixing of quantum states, i.e., $E(\sum_i p_i \sigma_i) \leq \sum_i p_i E(\sigma_i)$.

2.3 Entanglement measures

In the past few decades, a large number of entanglement measures have been introduced, including concurrence, logarithmic negativity, relative entropy of entanglement, entanglement cost, etc. For a detailed discussion, please see e.g. [8]. However, not all measures are computable for arbitrary dimensional systems. Below, we will briefly discuss a few bipartite and multipartite entanglement measures that we will utilize in this thesis.

2.3.1 Bipartite entanglement measures

Distance based entanglement measures: These are entanglement measures which are defined by taking into consideration the geometric structure of the state space. The set of separable states S_{AB} corresponding to a Hilbert space $\mathcal{H}_A \otimes \mathcal{H}_B$, is a closed convex set. The distance-based entanglement of a state ρ_{AB} on $\mathcal{H}_A \otimes \mathcal{H}_B$ is defined as the minimum distance of ρ_{AB} from the set S_{AB}, i.e.,

$$E(\rho_{AB}) = \min_{\sigma_{AB} \in S_{AB}} \mathcal{D}(\rho_{AB}, \sigma_{AB}). \tag{2.2}$$

Here, $\mathcal{D}$ is a function that we intend to use as a distance measure on the space of density operators on $\mathcal{H}_A \otimes \mathcal{H}_B$. Examples are the trace-norm, relative entropy, etc. We will discuss here about the relative entropy of entanglement in a little more detail.

Relative entropy of entanglement : This is a distance-based entanglement measure, where the distance used is the relative entropy between two states, which is defined as

$$S(\rho||\sigma) = \mathrm{Tr}\{\rho(\log_2 \rho - \log_2 \sigma)\}. \tag{2.3}$$

Note that $S(\rho||\sigma)$ is not symmetric with respect to σ and ρ. The relative entropy of entanglement is [23, 24]

$$E_{RE}(\rho_{AB}) = \min_{\sigma_{AB} \in S_{AB}} S(\rho_{AB}||\sigma_{AB}). \tag{2.4}$$

The relative entropy of entanglement also does not satisfy the triangle inequality. In Chap. 3, using the triangle inequality property of a distance measure, we will derive an entanglement-based bound on non-Markovianity. The corresponding distance measure, therefore cannot be the relative entropy of entanglement.

Negativity and logarithmic negativity: Using the PPT criterion, an entanglement measure called *negativity* ($\mathcal{N}$) can be identified. It is defined as the sum of the absolute values of negative eigenvalues of $\rho_{AB}^{T_A(T_B)}$ [25–29]. It can also be written as

$$\mathcal{N}(\rho_{AB}) = \frac{\|\rho_{AB}^{T_A}\| - 1}{2}, \tag{2.5}$$

where $\|A\| = \mathrm{Tr}\sqrt{A^\dagger A}$ is the matrix trace norm of A. Negativity is not additive, i.e. $\mathcal{N}(\rho_{AB}^{\otimes 2}) \neq 2\mathcal{N}(\rho_{AB})$, in general. Based on negativity, one can define an additive entanglement measure, called *logarithmic negativity (LN)*, and is given by [14, 15, 25, 28–30],

$$E_{LN}(\rho_{AB}) = \log_2(2\mathcal{N}(\rho_{AB}) + 1). \tag{2.6}$$

However, $E_{LN}(\rho_{AB})$ does not satisfy the convexity property. See [29] in this regard. But the advantage of these two measures is that, they are computable with relative ease for general (possibly, mixed) quantum states. But they cannot be used as entanglement measures of PPT states, as the corresponding value will always be zero. In Chap. 4, we will use *LN* as an entanglement measure of the state in any partition of a three-qubit "quantum refrigerator". In Chap. 5 we will use *LN* to calculate bipartite entanglement between two sites of a certain Hubbard Model and investigate its behaviour with changing inter-site distance and system parameters.

Concurrence: For two qubit states, the concurrence is a computable measure of en-

tanglement, and is defined as [31, 32]

$$C(\rho_{AB}) = \max\{0, \lambda_1 - \lambda_2 - \lambda_3 - \lambda_4\}. \tag{2.7}$$

Here, λ_i's are the square roots of eigenvalues, in decreasing order, of the matrix $\rho\tilde{\rho}$, where $\tilde{\rho} = (\sigma_y \otimes \sigma_y)\rho^*(\sigma_y \otimes \sigma_y)$ is the spin-flipped matrix, and σ_y is the Pauli spin operator. Concurrence is a function of entanglement of formation [33], and vice-versa, for two-qubit states. The squared concurrence satisfies the *monogamy inequality* for multiqubit states, which will be defined in the following subsection.

Quantum discord: Before moving over to multiparty entanglement measures, let us briefly mention a measure of nonclassical correlation, beyond the notion of entanglement [34–37]. There are two equivalent ways to expand the classical mutual information $H(X : Y)$ between two random variables X and Y. One is to write $H(X : Y) = H(X) + H(Y) - H(X, Y)$, where $H(X)$, $H(Y)$ and $H(X, Y)$ are the Shannon entropies of the probability distributions corresponding to X, Y and the joint distribution of X and Y. Another way is to write $H(X : Y) = H(X) - H(X|Y)$, where $H(X|Y)$ is a conditional entropy. The first one is usually generalized to the quantum domain by using the von Neumann entropy $S(\rho) = -\mathrm{Tr}(\rho \log_2 \rho)$ in place of whenever there appears a Shannon entropy, and thus obtaining the "quantum mutual information" [38–40]

$$I(\rho_{AB}) = S(\rho_A) + S(\rho_A) - S(\rho_{AB}), \tag{2.8}$$

for a bipartite quantum state ρ_{AB}. It has been argued that the second expression for $H(X : Y)$ can be quantized as

$$J(\rho_{AB}) = S(\rho_A) - S(\rho_{A|B}), \tag{2.9}$$

where $S(\rho_{A|B})$ is the quantum conditional entropy, given by

$$S(\rho_{A|B}) = \min_{\Pi_i^B} \sum_i p_i S(\rho_{A|i}). \tag{2.10}$$

Here $\{\Pi_i^B\}$ is a set of rank-1 measurement operators on B, $p_i = \mathrm{Tr}_{AB}(\mathbb{I}_A \otimes \Pi_i^B \rho_{AB} \mathbb{I}_A \otimes \Pi_i^B)$ is the probability of getting outcome "i", and $\rho_{A|i} = \mathrm{Tr}_B(\mathbb{I}_A \otimes \Pi_i^B \rho_{AB} \mathbb{I}_A \otimes \Pi_i^B)/p_i$ is the state corresponding to outcome i. $\mathbb{I}$ is the identity operator on the Hilbert space of subsystem A. In the quantum domain, $I(\rho_{AB})$ and $J(\rho_{AB})$ are not equivalent, and this "discrepancy" is interpreted as being present due to the existence of nonclassical correlations. The difference of these two quantities is called quantum discord ($\mathcal{D}$). Interestingly, quantum discord can be nonzero even for nonentangled states. We have used quantum discord in Chap. 4 to calculate bipartite quantum correlation between the partitions of a three-qubit quantum refrigerator.

2.3.2 Multipartite entanglement measures

Quantifying multiparty entanglement is still on a much more slippery ground than the bipartite scenario. Evidence for the added complexity is observed e.g. in [41], which shows that even for pure states, multiparty systems have inequivalent classes of states with respect to transformations under stochastic LOCC. Further evidence is provided e.g. in [42], which shows that for pure multiparty states, even in the asymptotic scenario, there exists states that cannot be necessarily transformed reversibly into two-party singlets. We focus here on computability of the measure, and define one that is computable for all pure states and quantifies genuine multisite entanglement. This measure however is difficult to compute for mixed multiparty states. We then define another that is based on the concept of monogamy of quantum correlations, and can be computable also for mixed multiparty states.

Generalized Geometric Measure: For an N-party pure quantum state $|\phi\rangle$, the gen-

eralized geometric measure (GGM) is a computable measure of genuine multisite entanglement, which is formally defined as the optimized fidelity-based distance of the state from the set of all pure states that are not genuinely multiparty entangled [43–46]. A multiparty pure state is said to be genuinely multiparty entangled if it is entangled across all bipartitions. Mathematically, the GGM can be evaluated as

$$\mathcal{G}(|\phi\rangle) = 1 - \lambda^2_{\max}(|\xi_N\rangle),$$

where $\lambda_{\max} = \max |\langle\xi_N|\phi\rangle|$, and $|\xi_N\rangle$ is an N-party non-genuinely multisite entangled quantum state and the maximization is performed over the set of all such states. The GGM can be effectively computed using the relation

$$\mathcal{G}(|\phi\rangle) = 1 - \max\{\lambda^2_{A:B}|A \cup B = A_1, \ldots, A_N, A \cap B = \phi\},$$

where $\lambda_{A:B}$ is the maximum Schmidt coefficient in an arbitrary bipartite split $A : B$ of the given state $|\phi\rangle$. A computational difficulty of the multiparty entanglement measure $\mathcal{G}$ lies in the fact that the number of possible bipartitions increases exponentially with an increase of the lattice size. In Chap. 5, we have used the GGM to calculate the multipartite entanglement in a Hubbard model with lattice sizes up to $N = 16$.

Monogamy score: A tripartite quantum state, ρ_{ABC}, is said to be monogamous under the bipartite quantum correlation measure Q, if $Q(\rho_{A:BC}) \geq Q(\rho_{AB}) + Q(\rho_{AC})$, where ρ_{AB} (ρ_{AC}) is obtained from ρ_{ABC} by tracing out C (B). Otherwise, the state is deemed as non-monogamous [47–49]. The "monogamy score" with respect to Q, for the three-party state, ρ_{ABC}, is defined as $\delta Q = Q(\rho_{A:BC}) - Q(\rho_{AB}) - Q(\rho_{AC})$. Positivity of δQ for a given quantum state, ρ, implies monogamous nature of the state ρ for the quantum correlation measure Q. The quantity δQ, has been argued to be a measure of multipartite correlation. Moreover, if the bipartite correlation measure Q is chosen as concurrence, then δQ can be computed for all pure multiqubit states [47]. Choosing the measure to be quantum

discord, renders it at least numerically computable, effectively for even mixed states of multiparty systems for low local dimensions [50].

Equipped with the relevant quantum correlation measures, we begin in the next chapter with an analysis of open system dynamics by proposing a new quantification of non-Markovian dynamics and deriving an entanglement-based bound on the corresponding non-Markovianity measure.

3

Almost Markovian maps and ϵ-nonmarkovianity

[1]In the introduction of this thesis, we have discussed how non-Markovian effects emerge in reduced dynamics of an open quantum system and looked at some examples of quantum information protocols where non-Markovinity can act as resource. Over the years, a number of non-Markovianity measures have been proposed. This includes a measure that identifies non-Markovianity by studying the time-dynamics of entanglement between the system and an auxiliary system [51]. A Markovian evolution causes monotonic decrease of the entanglement, whereas a non-Markovian evolution may give rise to consecutive decay and revival of the entanglement between system and auxiliary. This behavior of entanglement can be captured in the divisibility property of the dynamical map of the reduced system. Using the concept of divisibility of dynamical maps [52], Rivas *et al.* [51] formulated a necessary and sufficient criterion to detect non-Markovianity when the exact form of the dynamical map of the reduced system is known. Further studies in this direction include [53]. There are several works that looks for manifestation of non-Markovianity in the non-monotonic behaviour of a number of other quantum-mechanical properties of a system, e.g. flow of quantum Fisher information [54], fidelity difference [55], quantum mutual information [56], volume of accessible states of a system [57], accessible information [58], total entropy production [59], quantum interferometric power [60], coherence [61], etc. Another class of measures, proposed by Breuer *et al.* [62], associates

[1]This chapter is based on arXiv:1905.06198

the distinguishability of quantum states with the non-Markovian behavior of their evolution. A backflow of information from the environment to the system possibly increases the distinguishability, whereas in case of Markovian evolution, the one-way information flow from the system to the surroundings results in monotonic decrease of the distinguishability of the quantum states [63–65]. However, there are instances when these different non-Markovianity measures are not in agreement with each other. Specific examples show that the evolution of an open quantum system can be Markovian according to BLP but the corresponding dynamical map is indivisible and hence the evolution is non-Markovian according to RHP [66, 67]. Another work demonstrates that the BLP measure is not equivalent to a non-Markovianity meausure based on correlations [54, 68]. Though there has been attempts to correlate the different measures, a clear understanding and quantification of non-Markovianity and its relatively subtler issues have remained elusive.

In our work, we propose a distance-based measure of non-Markovianity which is independent of the above two characterizations (see [51] in this regard). With the usual picture of a system and its environment, we consider an additional bath (environment), which is much larger than the environment immediate to the system, and in which our system and environment are immersed. A set of maps, called ϵ-Markovian maps, are conceptualized, and ϵ-nonmarkovianity of a dynamical map is defined as the minimized distance of that map from the set of ϵ-Markovian maps. We derive an inequality which gives a bound on the above measure of non-Markovianity of a general dynamical map, in terms of an entanglement-like quantity. In the special case of $\epsilon = 0$, we obtain this bound on non-Markovianity in terms of an entanglement [69] of the system-environment joint state. Also, we numerically study the behavior of the non-Markovianity meausre for a amplitude damping channel and a phase damping channel, where, depending on the range of the respective parameters, the channels can behave as a Markovian or a non-Markovian map.

This chapter is organized as follows. In Section 3.1, we will review some existing measures of non-Markovianity. In Section 3.2, we will discuss the physical model we have considered in our work and will introduce the non-Markovianity measure, called the ϵ-nonmarkovianity. In Section 3.3, we will demonstrate numerical results showing the behaviour of ϵ-nonmarkovianity with time. Finally, in Section 3.4, we will derive the entanglement-based bout on our non-Markovianity measure, followed by a conclusion.

3.1 Measures of non-Markovianity

In this section, we will broadly discuss two classes of measure, which are- the RHP measure [51] and the BLP measure [62].

1. Rivas-Huelga-Plenio measure of non-Markovianity: In [51], Rivas *et. al.* showed that the non-Markovian nature can be detected by observing the non-monotonic temporal decay of entanglement between the open system and any other auxiliary system. They proposed a measure which detects this non-monotonic behaviour of entanglement, and put forward to a sufficient criterion to detect non-Markovianity from that measure. However, in the case, when the exact knowledge about the dynamical map is available, they were able to put forward a necessary and sufficient condition for non-Markovianity detection, which is based on the divisibility breaking of the dynamical map.

2. Breuer-Laine-Pillo measure of non-Markovianity: In [62], Breuer *et. al.* proposed a measure of non-Markovianity which takes into account the information backflow from environment to the system. Due to the one way information flow in Markovian dynamics, the distinguishability between two quantum states tends to monotonically decrease with time. But in non-Markovian dynamics, the information backflow can cause temporal increase in the distinguishability between the

quantum states. The measure given in [62], calculates non-Markovianity by measuring the total increase of distinguishability, in a fixed time interval.

3.2 The system-environment model and ϵ-nonmarovianity

In our work, we try to understand the concept of non-Markovianity and particularly try to find that in which realistic situations it is possible to arrive at Markovian limit of the dynamics of the reduced system. We propose a measure of non-Markovian behaviour, independent of the past formalisms used to measure non-Markovianity. We begin with the usual picture when a system S is in contact with an environment E. However, additional to that, the joint system SE is immersed in a much larger environment E_1. We denote the corresponding Hilbert spaces by $\mathcal{H}_S$, $\mathcal{H}_E$, and $\mathcal{H}_{SE}$. Initially, the total system SEE_1 is in a product state along the $S : EE_1$ bipartition, so that the reduced system SE is also a product state along the $S : E$ partition. With passing time, the total system evolves unitarily and becomes entangled across different partitions. The reason that we consider a larger environment E_1 in which the system-environment duo SE is immersed will become clear later when we discuss about Markovian-like maps. If we look at the reduced system SE, the time evolution can be described by the dynamical map Λ_{SE}. Thus, at any time t, the state of SE is

$$\rho^{SE}(t) = \Lambda_{SE}(\rho_0^S \otimes \rho_0^E), \tag{3.1}$$

where ρ_0^S and ρ_E^0 are the initial states of S and E.

Now we consider a particular subset of dynamical maps $\tilde{\Lambda}_{SE}^{\epsilon}$, such that that for any fixed $\epsilon \geq 0$, the time-evolved state $\tilde{\rho}^{SE}(t)$ satisfies the inequality

$$I_Q(\tilde{\rho}^{SE}(t)) \leq \epsilon, \qquad \forall\, t, \rho_0^S, \rho_0^E, \tag{3.2}$$

where $I_Q(\varrho^{AB}) = S(\varrho^A) + S(\varrho^B) - S(\varrho^{AB})$, is the quantum mutual information [70–73], of a

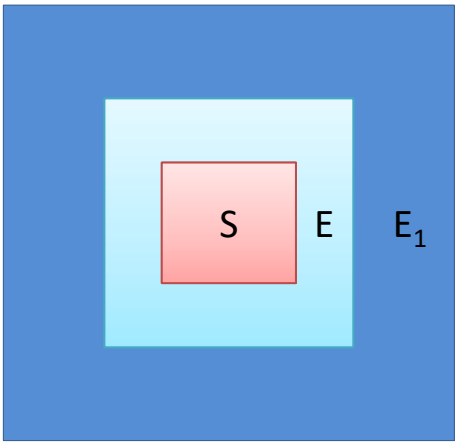

Figure 3.1: A schematic diagram showing the system S immersed in environment E. The joint system SE is in contact with a larger environment E_1.

bipartite state ϱ^{AB}, whereas ϱ^{A} and ϱ^{B} are respectively the reduced states of subsystems A and B, and $S(\cdot)$ is the von Neumann entropy of its argument. Note that the quantum mutual information is a non-negative quantity, so that $I_Q(\tilde{\rho}^{SE}(t))$ in inequality (3.2) is lower bounded by zero. If the above condition is satisfied, we will refer to the corresponding reduced maps $\tilde{\Lambda}_S^{\epsilon}$ of system S as ϵ-Markovian maps. The set of all such ϵ-Markovian maps is denoted by S^{ϵ}. Therefore, for the vanishing ϵ case, we have constrained our non-Markovian maps to lie within the set of non-divisible maps. See [74] in this regard.

Our goal is to quantify the non-Markovianity of a general dynamical map Λ_S by its distance $\mathcal{D}$ from the ϵ-Markovian maps $\tilde{\Lambda}_S^{\epsilon}$, minimized over the set S^{ϵ}. We call it ϵ-*nonmarkovianity* of the corresponding map Λ_S, and denote it by $N^{\epsilon}(\Lambda_S)$. That is,

$$N^{\epsilon}(\Lambda_S) = \min_{\tilde{\Lambda}_S^{\epsilon} \in S^{\epsilon}} \mathcal{D}(\Lambda_S \| \tilde{\Lambda}_S^{\epsilon}). \tag{3.3}$$

The distance $\mathcal{D}$ on the space of maps can be conceptualized in a variety of ways. Later on, we will use the Choi-Jamiołkowski-Kraus-Sudarshan (CJKS) isomorphism [75–77] to define it. Now however, we define it by a maximization over the density operators on

which the relevant maps act. More precisely, we define

$$\mathcal{D}(\Lambda||\Lambda') = \max_{\rho} \mathbf{D}(\Lambda(\rho)||\Lambda'(\rho)) \tag{3.4}$$

where $\mathbf{D}$ is a distance measure defined on the space of density operators, which forms the domain of the maps involved in $\mathcal{D}$. We therefore have

$$N^{\epsilon}(\Lambda_S) = \min_{\tilde{\Lambda}^{\epsilon}_S \in S^{\epsilon}} \max_{\rho^S_0} \mathbf{D}(\Lambda_S(\rho^S_0)||\tilde{\Lambda}^{\epsilon}_S(\rho^S_0)), \tag{3.5}$$

where we have involved ourselves in an additional maximization over all the initial states ρ^S_0. For a fixed $\tilde{\Lambda}^{\epsilon}_S$, if $\bar{\rho}^S_0$ is the state that maximizes $\mathbf{D}(\Lambda_S(\rho^S_0)||\tilde{\Lambda}^{\epsilon}_S(\rho^S_0))$, then

$$\mathbf{D}(\Lambda_S(\bar{\rho}^S_0)||\tilde{\Lambda}^{\epsilon}_S(\bar{\rho}^S_0)) \leq \mathbf{D}(\Lambda_{SE}(\bar{\rho}^S_0 \otimes \rho^E_0)||\tilde{\Lambda}^{\epsilon}_{SE}(\bar{\rho}^S_0 \otimes \rho^E_0)) \tag{3.6}$$

where we have assumed that the distance $\mathbf{D}$ satisfies the inequality $\mathbf{D}(\mathrm{tr}_p\sigma||\ \mathrm{tr}_p\varrho) \leq \mathbf{D}(\sigma||\varrho)$, where tr_p is partial trace over the system denoted by "p". Examples of such distances are trace-norm, relative entropy, etc. [78–80].

The measures of non-Markovianity and ϵ-nonmarkovianity depended, among other things, on the fact that we perform a maximization over the set of density matrices on the system S. See Eq. (3.4). Let us refer to this strategy as that of "max-distance". This however is hardly a unique strategy, and in particular, one can certainly define the distance between the maps by using a *minimization* over the density operators, i.e., by using the distance

$$\mathcal{D}_m(\Lambda||\Lambda') = \min_{\rho} \mathbf{D}(\Lambda(\rho)||\Lambda'(\rho)). \tag{3.7}$$

So, the definition of non-Markovianity accordingly changes to

$$N^{\epsilon}_m(\Lambda_S) = \min_{\tilde{\Lambda}^{\epsilon}_S \in S^{\epsilon}} \min_{\rho^S_0} \mathbf{D}(\Lambda_S(\rho^S_0)||\tilde{\Lambda}^{\epsilon}_S(\rho^S_0)). \tag{3.8}$$

We refer to this approach as that of the "min-distance".

Let us first consider the special case of $\epsilon = 0$. Consequently, the minimization in Eq. (3.3) will be over maps that lead to time-evolved states $\tilde{\rho}^{SE}(t)$ for which $I_Q(\tilde{\rho}^{SE}(t)) = 0$, $\forall t, \rho_0^S, \rho_0^E$. $I_Q(\rho^{AB}) = 0$ implies that the state ρ^{AB} is a product of individual states of the component systems. A product state for SE at all times for an initial product state of SE can appear in the following way.

The evolution of SEE_1 is unitary, which can be global (i.e., entangling), and hence, the entanglement and other classical and quantum correlations [37, 69, 81] that arise between S and EE_1 may remain between parts of S and parts of EE_1 or between the wholes (S and EE_1), unless the unitary is very special. However, it may so happen that the interaction between S and E is weaker (or equivalently, the information flow between S and E is slower) than that between E and E_1, so that any entanglement (or other correlations) created between S and E are transferred, and consequently hidden, in entanglement (or other correlations) between S and E_1. In other words, after an interaction between S and E, the state of E at a given time t, is quickly transferred into the recesses of E_1, and replaced with a ρ_0^E, which has no correlations with S, and this is done before the next interaction of E with S starts off. This is the Markovian-like limit in our scenario. Let us denote the set of all such reduced dynamical maps by S^0, and call them as Markovian-like.

3.3 Time-behaviour of ϵ-nonmarkovianity

3.3.1 Amplitude-damping channel

To exemplify the behavior of non-Markovianity, we consider a amplitude-damping channel [78, 82–86] having the Lindblad generator $\mathcal{L}(\rho(t))$ (see [85]) given by

$$\mathcal{L}(\rho(t)) = \sigma_-\rho(t)\sigma_+ - \frac{1}{2}\{\sigma_+\sigma_-, \rho(t)\}, \tag{3.9}$$

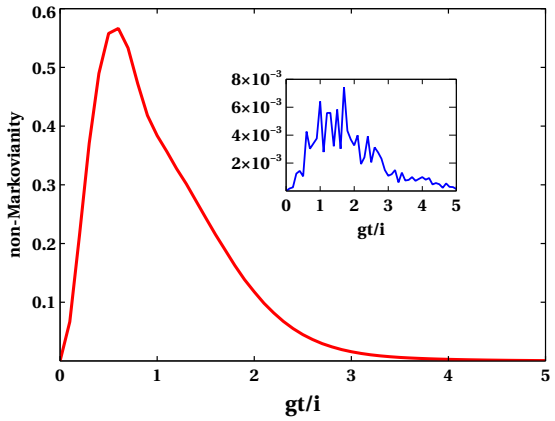

Figure 3.2: Non-Markovianity of the amplitude damping channel for the "max-distance" (red-solid curve) approach. We plot the non-Markovianity of the amplitude damping channel for $\lambda\kappa = 4$, $\gamma_0\kappa = 4$, where κ is a constant having the unit of time. Note that for such choice of $\lambda\kappa$ and $\gamma_0\kappa$, $g\kappa$ is purely imaginary. The horizontal axis represents gt/i, while the vertical one represents non-Markovianity for $\epsilon = 0$. Both axes are dimensionless. The distance between two density matrices is calculated by using the trace distance. The Haar-uniform searches are performed over 2000 values of the pair γ_0, and over 2000 density matrices, for each value of gt/i. In the inset, the blue solid curve is the non-Markovianity in "min-distance" approach, for the same choice of parameters. Note that the increased oscillations in the min distance approach is possibly a numerical artefact, and if we disregard them, the general trend of the curves for mi- and max-distance approaches are similar.

where σ_- and σ_+ are the qubit raising and lowering operators, and we are in the limit of a zero temperature bath. The corresponding master equation is $\dot{\rho} = \gamma_a(t)\mathcal{L}(\rho(t))$, where the time-dependent decay rate $\gamma_a(t)$ is given by

$$\gamma_a(t) = \frac{2\lambda\gamma_0 \sinh\frac{tg}{2}}{g\cosh\frac{tg}{2} + \lambda\sinh\frac{tg}{2}}, \quad g = \sqrt{\lambda^2 - 2\gamma_0\lambda}. \tag{3.10}$$

Depending on the values of the parameters $\{\gamma_0, \lambda\}$, the bath can behave as Markovian or non-Markovian. When $\lambda > 2\gamma_0$, the evolution is Markovian and when $\gamma_0 > \lambda/2$, the evolution is non-Markovian. The non-Markovian map Λ_S is constructed by choosing a particular pair of values of γ_0 and λ such that $\gamma_0 > \lambda/2$. Keeping the value of λ the same as that for the non-Markovian map, we generate a class of Markovian maps $\tilde{\Lambda}_S^0$, by randomly choosing γ_0, from a uniform distribution, while satisfying the condition $\lambda > 2\gamma_0$.

In parallel, we also generate the set of all density operators ρ_0^S on $\mathbb{C}^2$ by Haar-uniformly generating pure states on the larger Hilbert space $\mathbb{C}^2 \otimes \mathbb{C}^2$. The generation of the density matrices is therefore according to the "induced metric" [87, 88]. We now apply both the maps on the elements of this set of density operators to obtain the time evolved states $\Lambda_S(\rho_0^S)$ and $\tilde{\Lambda}_S^0(\rho_0^S)$, and maximize the trace distance between them over this set of density operators. The trace distance thus obtained, is further minimized over the set of Markovian maps generated by varying γ_0 for a fixed λ, with $\lambda > 2\gamma_0$. The entire optimization process is executed for different points on the t-axis. The data is presented in Fig. 3.2 as the red solid curve. It is important to mention here that the optimization is performed under the assumption that the optimal Markovian map for a given non-Markovian amplitude damping channel is attained within the class of Markovian amplitude damping channels. The obtained values therefore forms, in the worst-case scenario, upper bounds of the actual values.

3.3.2 Phase-damping channel

Besides the amplitude-damping channel, we also want to investigate how $N^\epsilon(\Lambda_S)$ behaves during evolution through a phase damping channel. The master equation of the phase damping channel is [78, 89–91]

$$\frac{d\rho}{dt} = \frac{1}{2}\gamma(t)[\sigma_z\rho(t)\sigma_z - \rho], \tag{3.11}$$

where σ_z is the Pauli z-matrix. The time-dependent dephasing rate, $\gamma(t)$, is given by

$$\gamma(t) = \int d\omega J(\omega) \coth(\hbar\omega/2k_BT) \sin(\omega t)/\omega, \tag{3.12}$$

where the integration is over the frequency of the bath-modes denoted by ω, $J(\omega)$ is the spectral function of the bath. If we take our bath of consideration to have Ohmic-like

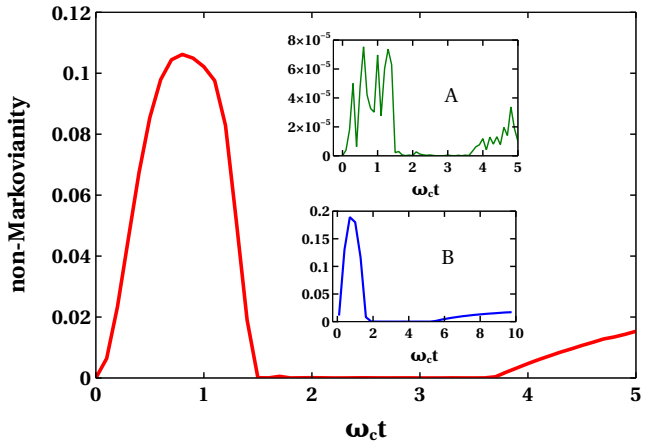

Figure 3.3: Non-Markovianity of the phase damping channel with respect to time t for "max-distance" (red-solid curve) approach, where $s_{NM} = 2.5$. The non-Markovianity decays, remains zero for finite interval, and then revives again. Inset:(A) Non-markovianity of the phase damping channel for "min-distance" approach when $s_{NM} = 2.5$. (B) Non-Markovianity of the phase damping channel in "max-distance" approach when $s_{NM} = 2.8$. Both the decay and revival occurs at later times compared to the case when $s_{NM} = 2.5$.

spectra, then the spectral function is

$$J(\omega) = \frac{\omega^s}{\omega_c^{s-1}} e^{-\omega/\omega_c}, \tag{3.13}$$

where ω_c is the frequency cut-off, and s is the Ohmicity parameter, which decides whether the bath will be Ohmic ($s = 1$), sub-Ohmic ($s < 1$), or super-Ohmic ($s > 1$). Keeping attention at the absolute zero temperature limit, we get the following expression for the dephasing rate:

$$\gamma_0(t) = \omega_c[1 + (\omega_c t)^2]^{-s/2}\Gamma(s)\sin[s\arctan(\omega_c t)] \tag{3.14}$$

In [91], P. Haikka *et al.* have demonstrated that the non-Markovianity behavior, of this channel, is observed only when $s > 2$. To numerically study $N^{\epsilon}(\Lambda_S)$ for a non-Markovian map, we take a particular value of $s = s_{NM}$, such that $s_{NM} > 2$, corresponding to the map Λ_S. We generate 2000 values of $s = s_M$ in the interval $0 < s < 2$, each corresponding to a Markovian map, and for each s_M, we Haar-uniformly generate 2000 random density matrices. the data is presented in Fig. 3.3 with respect to the $\omega_c t$ along the horizontal axis.

3.3.3 The CJKS approach to non-Markovianity.

In the analysis until now, we have defined distance on the space of maps by using a distance on the space of density operators on which the maps act and a corresponding double optimization. See Eqs. (3.4) and (3.7). However, instead of using these approaches (viz., the "max-distance" and the "min-distance" ones), in Eq. (3.3), we may define the distance on the space of maps on S by using the CJKS representation in the following way. We define

$$\mathcal{D}(\Lambda||\Lambda') = \mathbf{D}(\mathbf{I}\otimes\Lambda(|\Psi^+\rangle\langle\Psi^+|)||\mathbf{I}\otimes\Lambda'(|\Psi^+\rangle\langle\Psi^+|)) \tag{3.15}$$

where $|\Psi^+\rangle = \frac{1}{\bar{d}^{\frac{1}{2}}}\sum_{i=0}^{\bar{d}-1}|ii\rangle$, and $\mathbf{I}$ is the identity map on the space of operators on a "reference" Hilbert space, H_R, which has the same dimension $\bar{d}$, as H_S. Note that $|\Psi^+\rangle$ is an element of $H_R\otimes H_S$. This approach inherits the properties of the CJKS representation, and in particular has the benefit of a reduced level of optimization, as compared to the preceding approach. In Fig. 3.4, we provide a numerical calculation to exemplify the behavior of the non-Markovianity when seen through this approach, for the amplitude damping channel.

3.4 Entanglement-based bound on ϵ-nonmarkovianity

Going back to the scenario of general channels, but still remaining with the case when $\epsilon = 0$, we have

$$\mathbf{D}(\Lambda_{SE}(\bar{\rho}_0^S\otimes\rho_0^E)||\tilde{\Lambda}_{SE}^0(\bar{\rho}_0^S\otimes\rho_0^E)) \geq E(\Lambda_{SE}(\bar{\rho}_0^S\otimes\rho_0^E)), \tag{3.16}$$

where E is a distance-based entanglement defined as the minimum distance of a state from the set of separable states [69]. The inequality (3.16) holds by virtue of the fact that

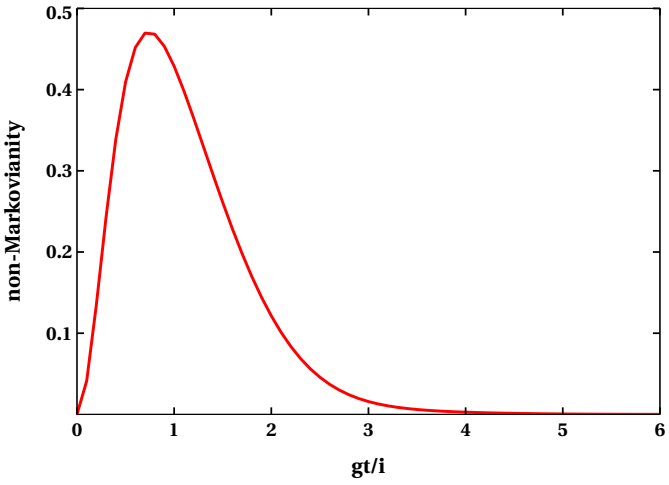

Figure 3.4: Non-Markovianity of the amplitude damping channel in the CJKS approach for $\lambda\kappa = 4$, $\gamma_0\kappa = 10$, The notations in this figure remain the same as in Fig. 3.2, except that the non-Markovianity is defined here from the CJKS approach, and that the curve is plotted by simply joining the data points.

$\tilde{\Lambda}^0_{SE}(\bar{\rho}^S_0 \otimes \rho^E_0)$ is a separable and indeed a product state. In case the distance **D** is the relative entropy on the space of density operators, E is the relative entropy of entanglement [24, 92] of its argument. Let us now assume that **D** satisfies the triangle inequality, which is in fact not satisfied by relative entropy distance. We then obtain

$$\mathbf{D}(\Lambda_{SE}(\bar{\rho}^S_0 \otimes \rho^E_0) \| \tilde{\Lambda}^0_{SE}(\bar{\rho}^S_0 \otimes \rho^E_0)) \leq E(\Lambda_{SE}(\bar{\rho}^S_0 \otimes \rho^E_0)) + d, \tag{3.17}$$

where d is the "diameter" of the convex set of separable states [25]. The diameter, d, of a set $\mathcal{S}$, is defined as

$$d(\mathcal{S}) = \max_{\rho,\sigma \in \mathcal{S}} \mathbf{D}(\rho, \sigma) \tag{3.18}$$

A geometric representation of the relation (3.17) is given in Fig. 3.5. By combining relations (3.6) and (3.17) with definitions (3.3) and (3.5), we have

$$N^0(\Lambda_S) \leq E(\Lambda_{SE}(\bar{\rho}^S_0 \otimes \rho^E_0)) + d. \tag{3.19}$$

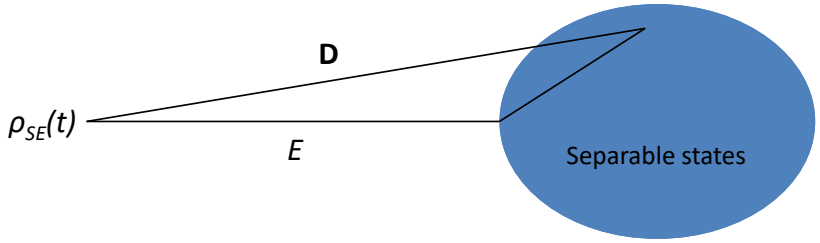

Figure 3.5: Geometric representation of the inequality between non-Markovianity and system-environment entanglement. We consider the case of $\epsilon = 0$. The shaded region represents the convex set of states that are separable in the system-environment bipartition. The optimal state that attains the optimization in the definition of non-Markovianity is on or inside the set of separable states. The distance of this state to the time-evolved state $\rho_{SE}(t)$ must be greater than the sum of the other two sides of the triangle depicted in the figure. These latter sides however are respectively a distance-based entanglement of the evolved state and a bound on the diameter of the set of separable states. We have assumed that the distance measure on the space of density matrices satisfies the triangle inequality.

This relation is true for all extensions of Λ_S into Λ_{SE} and for all ρ_0^E. Consequently,

$$N^0(\Lambda_S) \leq \min_{\rho_0^E, \Lambda_{SE}} [E(\Lambda_{SE}(\bar{\rho}_0^S \otimes \rho_0^E)) + d], \tag{3.20}$$

where the minimization is over all ρ_0^E and over all extensions of Λ_S into Λ_{SE}. Note that the diameter d is inside the optimization process, and not independent of it.

We now consider the general case, i.e., when $\epsilon \neq 0$. In this case, the time evolved state $\tilde{\rho}^{SE}(t) = \tilde{\Lambda}^{\epsilon}_{SE}(\bar{\rho}_0^S \otimes \rho_0^E)$ is no longer a product state, and instead it satisfies the inequality $I(\tilde{\Lambda}^{\epsilon}_{SE}(\bar{\rho}_0^S \otimes \rho_0^E)) \leq \epsilon$, a weaker condition, that does not require the argument to be product (for $\epsilon \neq 0$). The set of all states η^{SE} that satisfy $I_Q(\eta^{SE}) \leq \epsilon$ does not form a convex set; however the set of convex combinations of all such states is of course a convex set and we call this set as the set of ϵ-*separable* states. For $\epsilon = 0$, this becomes the usual set of separable states. We now minimize the distance of $\Lambda_{SE}(\bar{\rho}_0^S \otimes \rho_0^E)$ from the set of ϵ-separable states, and call it the ϵ-*entanglement*, E^{ϵ}, of the state $\tilde{\rho}^{SE}(t)$. If d_{ϵ} is the diameter

of the set of ϵ-separable states, we get the following inequality:

$$\mathbf{D}(\Lambda_{SE}(\bar{\rho}_0^S \otimes \rho_0^E)||\tilde{\Lambda}_{SE}^{\epsilon}(\bar{\rho}_0^S \otimes \rho_0^E)) \leq E^{\epsilon}(\Lambda_{SE}(\bar{\rho}_0^S \otimes \rho_0^E)) + d_{\epsilon}. \tag{3.21}$$

In this case, the relation (3.20) is replaced by

$$N^{\epsilon}(\Lambda_S) \leq \min_{\rho_0^E, \Lambda_{SE}} [E^{\epsilon}(\Lambda_{SE}(\bar{\rho}_0^S \otimes \rho_0^E)) + d_{\epsilon}]. \tag{3.22}$$

Considering the min-distance approach, suppose that for a fixed $\tilde{\Lambda}_S^{\epsilon}$, $\bar{\bar{\rho}}_0^S$ is the state that minimizes $\mathbf{D}(\Lambda_S(\rho_0^S)||\tilde{\Lambda}_S^{\epsilon}(\rho_0^S))$. Proceeding as in the case of "max-distance", we can see that in the special case of $\epsilon = 0$, the relation (3.17) changes to

$$\mathbf{D}(\Lambda_{SE}(\bar{\bar{\rho}}_0^S \otimes \rho_0^E)||\tilde{\Lambda}_{SE}^{0}(\bar{\bar{\rho}}_0^S \otimes \rho_0^E)) \leq E(\Lambda_{SE}(\bar{\bar{\rho}}_0^S \otimes \rho_0^E)) + d. \tag{3.23}$$

Accordingly, the relation (3.20) changes to

$$N_m^0(\Lambda_S) \leq \min_{\rho_0^E, \Lambda_{SE}} [E(\Lambda_{SE}(\bar{\bar{\rho}}_0^S \otimes \rho_0^E)) + d], \tag{3.24}$$

where the entanglement function is the same as before, while the actual quantity has changed to $E(\Lambda_{SE}(\bar{\bar{\rho}}_0^S \otimes \rho_0^E))$, in contrast to $E(\Lambda_{SE}(\bar{\rho}_0^S \otimes \rho_0^E))$ in the "max-distance" case.

The $\epsilon \neq 0$ can be similarly derived. It is important to stress here that despite the similarity of notation and the algebra, we have here a completely independent bound on an independent measure of non-Markovianity of a general dynamical map Λ_S, as compared to the case of "max-distance". Similar to the case of "max-distance", here also, we have numerically studied the behavior of non-Markovianity for the amplitude damping channel. This is presented in the inset of Fig. 3.2.

To conclude, we have considered a measure of non-Markovianity of a dynamical map on an open quantum system based on the distance of the dynamical map from the set

of all Markovian dynamical maps on the same system. We found a quantitative relation between the measure, and the entanglement between the reduced system and the environment. This relation can be used to estimate one of the quantities if we are able to find the other. To exemplify the notion and the relation, we have studied amplitude damping and phase damping channels. The ϵ-nonmarkovian maps can be realized experimentally in the laboratory set-ups which has been used for studying non-Markovian effects. One would need to perform tomogarphy of the quantum states and processes involved in the set-up to detect and measure ϵ-nonmarkovianity. A measurement of system-environment entanglement can provide an upper bound on the ϵ-nonmarkovianity.

4

Necessarily transient quantum refrigerator

[1]Study of the thermodynamic properties of microscopic quantum systems has been an active field of research in recent times [93–107]. Considerable efforts have been directed to develop and characterize quantum heat engines, and to determine whether "quantum" advantages can be obtained in these machines over their classical counterparts [108]. Quantum analogs of the well-known classical Carnot and Otto engines have been extensively studied [109–117], and implemented in laboratories using mesoscopic substrates [118], superconducting qubits [119], and ion systems [120].

On one hand, this has motivated researchers to test the laws of thermodynamics at the quantum mechanical level [106, 121–131], and to determine the efficiencies of quantum heat engines, analogous to those provided by the extensively studied classical heat engines [132–138]. On the other hand, a great deal of interest has been attracted towards building "small" quantum engines, like quantum refrigerators, which consist of only a few quantum levels, and the energy required to drive the refrigerator is obtained from local heat baths attached to the subsystems constituting the refrigerator, known as the absorption refrigerator [139–145]. Despite their simple working principles, small quantum refrigerators are shown to be useful in quantum error correction, where cold auxiliary qubits are considered as resources [146]. Implementation schemes for such models in laboratories [147, 148] have also been proposed, and realization of a three-qubit quantum

[1]This chapter is based on Europhys. Lett. **125**, 20007 (2019)

absorption refrigerator in trapped-ion systems has been possible [149]. The motivation for studying such microscopic refrigerators from an information-theoretic perspective [145] lies, for example, in the fact that thermodynamics has a close connection with both classical and quantum information theory [150, 151].

A special phenomenon, namely, the "steady-state cooling", in the case of a quantum self-sufficient refrigerator constituted of only three qubits [139–145] has recently been in focus. Here, the steady state temperature of one of the qubits, called the "cold" qubit, is less than its initial temperature, and it, in general, can occur at large time in the dynamics. However, refrigeration at short time in these models, which can be more accessible in the experiments, remains a relatively less explored topic. Only recently, a few studies have addressed this issue [143, 145], and pointed out the benefit of transient cooling over the steady state cooling, by using uncorrelated product thermal states as well as states with coherence in the energy eigenbasis, as the initial states. It has been shown that the transient regime of such refrigerators may provide a better cooling, in the sense of attaining a lower temperature, as compared to that in its steady state, which highlights the importance of the study of the systems as it approaches towards its equilibrium. In situations where the time scale to attain the equilibrium is too high to implement, or where very fast cooling is required, transient cooling may emerge as the *practical* and advantageous option to attain refrigeration. In [149], the authors have experimentally realized a three-qubit refrigerator by using trapped Ytterbium ions, where they have been able to observe the steady-state, as well as a transient cooling. In this paper, we ask the following question: *Can there exist a situation where the transient cooling is the "only" option for refrigeration to occur?* In such a scenario, no, or almost no steady-state cooling would take place. Our work answers the question affirmatively by using two different models of thermalization.

Towards this aim, we consider two paradigmatic models of thermalization for a three-qubit self-contained quantum refrigerator attached to local heat baths. One of them is

the well-studied reset model [140], and the other one is a more realistic scenario where the local baths are collections of harmonic oscillators that interact with the qubits via memoryless interactions [145]. We identify a *canonical* form of the qubit-bath interaction parameters which eases the presentation of situations where no steady-state cooling takes place, and transient cooling is the only option to attain refrigeration. We demonstrate this phenomenon for both the models, and find out regions in the space of the qubit-bath parameters where such a phenomenon takes place. We comment on the cooling power and coefficient of performance of the transient refrigerator, and show how the performance of the transient refrigerator in the absence of steady-state refrigeration can be modulated by tuning the temperature of the hottest bath. Moreover, we discuss the robustness of the phenomenon of transient refrigeration without steady-state refrigeration against the onslaught of a small perturbation to the qubit-bath interaction parameters, in canonical form.

We point out that with a modification of our canonical form of the qubit-bath interactions, a condition emerges where the system cools fast and attains its minimum temperature either at the steady state, or in the transient regime. For each set of parameters, we quantify the speed of cooling by introducing a "half-time", which the system takes to attain half the maximum cooling possible for the fixed set of parameters. Moreover, we discuss the behavior of the bipartite and multipartite quantum correlations in the three-qubit system, during the initial phase of the dynamics, over regions of the parameter space where transient cooling is the only option for refrigeration. Although the models of thermalizations considered in this chapter are of two different kinds, the results remain qualitatively unchanged in both the models. Interestingly, for the model of thermalization involving collections of harmonic oscillators as local bath, a "freezing", i.e., almost invariance, of the minimum temperature attained of the cold qubit with respect to change in system parameters is observed.

We have already presented a discussion on the open quantum dynamics of a system

interacting with its environment in Chapter 1. In the current chapter, the three qubits constitute the open system and each thermal bath acts as the environment of the corresponding qubit. The role of the environment in this case, is to provide free energy for the functioning of the refrigerator.

The chapter is organized as follows. In Section 4.1, we discuss the necessarily transient self-contained three-qubit quantum absorption refrigerator with two specific models of thermalization. While subsection 4.1.1 deals with the reset model of thermalization, a more realistic model with local heat-baths constituted of harmonic oscillators is presented in subsection 4.1.2. In Sec. 4.2, we discuss the properties of bipartite as well as multipartite quantum correlations in the system of three-qubits under the qubit-bath interactions corresponding to both the models discussed in this chapter. Sec. 4.3 contains the concluding remarks.

4.1 Three-qubit quantum absorption refrigerator

We consider a quantum absorption refrigerator consisting of three qubits [139, 143] labeled as "1", "2", and "3". The first qubit, "1", represents the qubit which is to be cooled, while "2" and "3" behave as the refrigerator. Describing the qubits in terms of standard Pauli representations, $\sigma_i^{x,y,z}$, where $\{|0\rangle, |1\rangle\}$, the eigenvectors of σ^z, forms the computational basis, the free Hamiltonian of the three-qubit system can be written as

$$\tilde{H}_{loc} = \frac{k}{2} \sum_{i=1}^{3} E_i \sigma_i^z, \tag{4.1}$$

where the ground and excited state energies of the qubit i are given by $-\frac{E_i}{2}$ and $\frac{E_i}{2}$, respectively, and k is a constant having the dimension of energy. The coupling between the qubits is represented by a three-body interaction Hamiltonian,

$$\tilde{H}_{int} = kg(|010\rangle\langle 101| + h.c.), \tag{4.2}$$

with kg being the corresponding interaction strength. Each of the qubits is considered to be weakly interacting with a heat bath at temperature $\tilde{T}_i$, where $\tilde{T}_1 \leq \tilde{T}_2 < \tilde{T}_3$. The interaction Hamiltonian H_{int} is such that, when qubit "1" and "3" jumps from excited state to ground state, qubit "2" absorbs the released energy and jumps to excited state from ground state. To make this process energy conserving, we assume $E_2 = E_1 + E_3$. The reverse process, i.e. $|010\rangle \rightarrow |101\rangle$ can also take place. However, cooling qubit "1" requires increasing its ground state probability, hence we need to bias H_{int} towards the transformation $|010\rangle \rightarrow |101\rangle$. This can be achieved if initially the probability of the eigenstate $|010\rangle$ is greater than that of $|101\rangle$. That is why the third qubit is coupled with the hottest bath, while the bath associated with the second qubit is considered to be at room temperature. We assume that the interactions between the qubits are switched on at time $\tilde{t} = 0$, such that $kg \geq 0$ for $\tilde{t} > 0$. All the qubits are initially in a thermal equilibrium state with their respective baths, and the initial state of the three-qubit system is given by $\rho_0 = \rho_0^1 \otimes \rho_0^2 \otimes \rho_0^3$, with

$$\rho_0^i = \frac{1}{Z_i} \exp(-\tilde{\beta}_i k E_i \sigma_i^z/2). \tag{4.3}$$

Here, $Z_i = \mathrm{Tr}\left[\exp(-\tilde{\beta}_i k E_i \sigma_i^z/2)\right]$ is the partition function corresponding to the qubit i, and $\beta_i = (k_B \tilde{T}_i)^{-1}$, k_B being the Boltzmann constant.

The dynamics of the entire three-qubit system, controlled by the choice of the system parameters as well as the parameters corresponding to the system-bath interaction, drives the system to a time-evolved state $\rho(t)$, which is obtained as a solution of the master equation

$$\frac{\partial \rho}{\partial \tilde{t}} = -\frac{i}{\hbar}[\tilde{H}_{loc} + \tilde{H}_{int}, \rho] + \Phi(\rho). \tag{4.4}$$

Eq. (4.4) governs the dynamics of the three-qubit system, where the operator Φ depends solely on the type of the local reservoirs attached to the qubits, and the type of interaction

between the qubits and the reservoirs. Let us now re-write the dynamical equation in dimensionless variables and parameters as

$$\frac{\partial \rho}{\partial t} = -i[H_{loc} + H_{int}, \rho] + \frac{\hbar}{k}\Phi(\rho), \tag{4.5}$$

where $t = k\tilde{t}/\hbar$, $H_{loc} = \tilde{H}_{loc}/k$, and $H_{int} = \tilde{H}_{int}/k$. The second term on the right-hand-side will be written in dimensionless form after an explicit definition of $\Phi(\rho)$, to be given later. Let us also introduce the dimensionless parameter $T = k_B/k$ times the absolute temperature, so that the initial state of the ith qubit is

$$\rho_0^i = \frac{1}{Z_i}\exp(-E_i\sigma_i^z/2T_i). \tag{4.6}$$

The transient temperature, $T_c(t)$, of the cold qubit (i.e., the qubit to be cooled, which is qubit "1") is determined by using Eq. (4.3), from the local density matrix $\rho^1(t)$ corresponding to the cold qubit, obtained by tracing out qubits 2 and 3 from $\rho(t)$. Note here that $T_c(t)$ is a function of the system parameters and the parameters corresponding to the qubit-bath interactions also. If $T_c(t) < T_1$ at some specific value of t, we call it to be a successful cooling of the qubit "1" with the help of the refrigerator, i.e., qubits "2" and "3". Let us denote the steady state temperature of the cold qubit by T_1^s, which corresponds to the steady state of the system, given by $\partial\rho/\partial t = 0$. We call a situation to be of steady state cooling (SSC) if $T_1^s < T_1$, while $T_c(t) < T_1$ represents a case of transient cooling (TC) at time t.

We now discuss the occurrence of SSC and TC in two different scenarios. The scenarios differ by the choices of the heat baths and the types of qubit-bath interactions. Unless otherwise mentioned, in both the cases, we consider $E_1 = 1$, and $T_1 = 1$. We take $T_2 = T_1$, implying a scenario where the cold qubit is initially at room temperature, like the second qubit. We further set $E_2 = E_1 + E_3$. Note here that $[H_{loc}, H_{int}] = 0$, so that in the closed evolution, the interaction and the field energies are separately conserved. Note that the

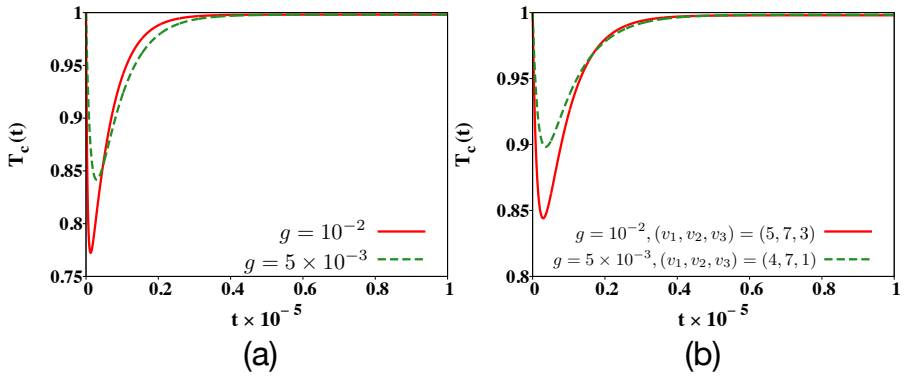

Figure 4.1: (a) Necessarily transient reset model refrigerator. We plot the variation of $T_c(t)$ as a function of t for $g = 10^{-2}$ and 5×10^{-3}, where the values of (x, y) are set at $(3.5, 2.5)$. (b) **Robustness of CIP in the reset model.** We plot the variation of temperature of the cold qubit as a function of time, for different perturbations. The set of qubit-bath interaction parameters, $\{p_i\}$, are modified to $\{p_i + u_i \times 10^{-v_i}\}$, where $u_i = 1$, $i = 1, 2, 3$, $(v_1, v_2, v_3) = (5, 7, 3)$ for $g = 10^{-2}$, and $(v_1, v_2, v_3) = (4, 7, 1)$ for $g = 5 \times 10^{-3}$. All quantities are dimensionless.

initial state, ρ_0, is diagonal in the eigenbasis of H_{loc}, and the only off-diagonal elements emerging in the evolved state due to H_{int} are $|010\rangle\langle 101|$ and its hermitian conjugate. The qubit-bath interactions do not generate coherence between the eigenbasis elements of the individual qubits, thereby keeping the form of $\rho(t)$ unchanged. Thus, it leads to diagonal local density matrices corresponding to each qubit, obtained by tracing out the other two qubits from $\rho(t)$. This allows one to define a local temperature for the cold qubit at every time instant t, according to Eq. (4.6).

4.1.1 Reset model

The first example that we consider deals with the representation of the qubit-bath interaction via a simple "reset model" [140], where at every time step, a probabilistic *reset* occurs to the state of each of the three qubits. With a high probability, the state of qubit i is left unchanged, while in the rest of the situations, the qubit is reset to the initial thermal

state ρ_0^i. Hence the operator Φ, in this case, is given by

$$\Phi(\rho) = \sum_{i=1}^{3} \tilde{p}_i(\varphi_i(\rho) - \rho), \tag{4.7}$$

where $\{\tilde{p}_i\}$ are the probability densities per unit time, and $\varphi_i(\rho) = \rho_0^i \otimes \mathrm{Tr}_i(\rho(t))$. We now introduce the dimensionless parameter, $p_i = \frac{\hbar}{k}\tilde{p}_i$, thus resulting in a dimensionless second term in the right-hand-side of the dynamical equation (4.5). For such a qubit-bath interaction, the master equation given in Eq. (4.5) can be applied in the perturbative regime, where $g, p_i \ll E_1, E_3$ [140]. Solving the quantum master equation, for fixed values of the system parameters, the steady state temperature and the transient temperature of the cold qubit, as a function of time, can be computed. It has been observed that for $g > p_i$, $i \in \{1, 2, 3\}$, $T_c(t)$ initially oscillates with an approximate frequency g/π. This is because, at initial times, a large value of g implies that the inter-qubit interaction dominates the evolution, and hence a better cooling of the cold qubit takes place. At larger times, the dissipation starts to dominate, and the system approaches to its steady state [143]. Typically, the time taken (in units of the dimensionless parameter, t) for the dissipative dynamics to damp out the oscillations was found to scale as q where $q^{-1} = \sum p_i$. Thus, for specific values of the parameter g and the probabilities, $\{p_i\}$, it has been shown that the temperature of the cold qubit in the transient regime can be lower than that of the steady state, i.e., one can have situations for which $T_c(t) < T_1^s$. This implies that, in those parameter regions, the refrigerator can be more effective in the transient domain compared to being in the steady state. In this paper, we wish to find out the parameter region in which TC occurs without any SSC. Specifically, we are now interested in the scenario where $T_c(t) < T_1^s = T_1$.

Canonical qubit-bath interaction parameters. We propose a *canonical* form of a set of qubit-bath interaction parameters, $\{\kappa_i\}$, as

$$\kappa_1 = 10^{-x},\ \kappa_2 = 10^{-(x+y)},\ \kappa_3 = 10^{-(x-y)}, \tag{4.8}$$

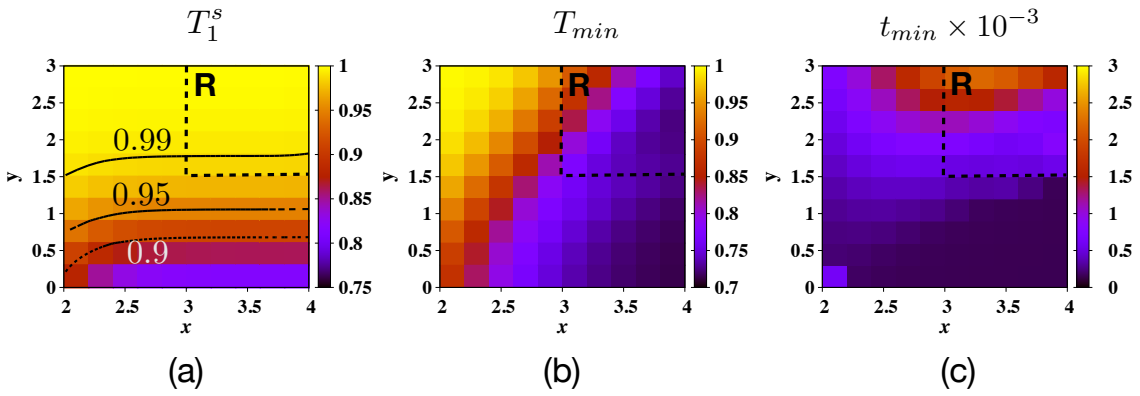

Figure 4.2: Thermodynamic system characteristics in the reset model on the CIP plane. We present the projection-plots of (a) T_1^s, (b) T_{min}, and (c) t_{min} as functions of x (horizontal axis) and y (vertical axis) for $g = 10^{-2}$. The continuous lines in the graph (a) correspond to $T_1^s = 0.9, 0.95, 0.99$ (from bottom to top). The first quadrants of the figures, where copious occurrences of TC without SSC are found, are marked by "**R**" and bounded by the dashed lines. All quantities are dimensionless.

where $x, y \geq 0$, such that $\max\{\kappa_1, \kappa_2, \kappa_3\} = \kappa_3$, and $\kappa_i \leq 1$. We refer to the choice of the parameters according to Eq. (4.8) as the canonical qubit-bath interaction parameters (CIP). The proper choices of x and y dictates the values of $\{\kappa_i\}$. For example, the dimensionless qubit-bath interaction parameters $\{p_i\}$ in the reset model can be chosen according to Eq. (4.8). We shall show that such a choice of $\{p_i\}$ will finally lead to the TC without the SSC. However, the choice of the values of x and y have to be made in such a way that the master equation remains valid. We will see later that such choice of these parameters can be useful in other models also, discussed in the succeeding subsection.

Refrigeration in a necessarily transient regime. We demonstrate the usefulness of CIP in characterizing the necessarily transient three-qubit quantum absorption refrigerator in the case of the present model. This corresponds to a scenario where the qubit-bath coupling corresponding to the hot qubit is the strongest, while that of the intermediate qubit is the weakest. Since the intermediate qubit is the one dissipating energy into the environment, a weak coupling of this qubit with the heat-bath may lead to a high steady-state temperature, while transient cooling can still be achieved in this regime.

Let us consider $x = 3.5$ and $y = 2.5$, such that $p_3 = 10^{-1}$, and $p_2 < p_1, p_3$. The rest

of the system parameters are set at $E_3 = 10^2$ and $T_3 = 10^2$. The variation of $T_c(t)$ as a function of t for different values of g are shown in Fig. 4.1(a). The temperature of the cold qubit (qubit "1") decreases at first, reaches a minimum, and then increases to attain a steady state at a temperature $T_1^s \approx T_1$, i.e., for the cold qubit, the steady state temperature is approximately the same as the initial temperature. Such phenomena can be observed by tuning the system parameters and the qubit-bath interaction parameters, as shown in Fig. 4.1(a). It is clear that in scenarios like this, cooling in the steady state is negligible, while substantial cooling occurs in the transient regime. Therefore, the three-qubit system represents a *necessarily* transient quantum absorption refrigerator, since the only way of obtaining the cold qubit at a temperature lower than T_1 is to halt the dynamics at a time t in the transient regime, i.e., when $T_c(t) < T_1$. In other words, there exist points in the parameter space, where, if the experimentalist finds herself/himself forced to work in, due to may be some practical limitations in the laboratory technology, the only way to have a refrigerator, within the reset model, is to consider a transient regime cold qubit. Note here that the values of the system parameters, given by $\{E_i\}, \{T_i\}$, and g, are chosen to be similar to those used in Refs. [139, 143], where the occurrence of both TC and SSC was reported. This allows us to compare our results with the cooling phenomena reported in Refs. [139, 143]. This also implies that the occurrence of TC without SSC can be achieved by tuning the qubit-bath interaction parameters, while keeping the system parameters in the same domain as in Refs. [139, 143].

Note here that in the case of a good absorption refrigerator with SSC, it is desired that the object to be cooled should be well-insulated. Hence, the coupling of the first (cold) qubit with the environment should be taken to be small. It is also needed that the intermediate qubit (qubit 2), the one dissipating energy into the environment, interacts with the environment strongly, to dissipate heat quickly, implying a high value of the interaction parameter corresponding to qubit 2 and its environment. We point out here that the phenomenon of TC without SSC, according to Eq. (4.8), corresponds to strongest coupling between the hot qubit and its environment, i.e., the highest value amongst $\{\kappa_i, i =$

$1, 2, 3\}$ is that of κ_3, and the weakest coupling between the intermediate qubit and its environment, i.e., the lowest value among the same is of κ_2.

A weak coupling of the intermediate qubit with its heat-bath may lead to a high steady-state temperature. However, the interaction among the three qubits (as quantified by g) drives them away from the respective thermal states, providing transient cooling. That a transient cooling happens for short time scales instead of a transient heating in our case where there is no coherence in the initial state, is due to the specific choice of the population ratio of the energy levels $|010\rangle$ and $|101\rangle$ in the initial state, which in turn is fixed by the choice of the energies and temperatures in the system. Due to higher coupling of the first and third qubits with their environments, they tend to come back to the initial thermal states more quickly. On the other hand, the second qubit remains relatively more insulated and thus fails to act as a good energy dissipator. Therefore, after sufficiently long time, there occurs no significant cooling of the first qubit though substantial transient cooling can be achieved.

Robustness. The next question is whether the phenomena of transient refrigeration without the steady state refrigeration, when the qubit-bath interaction parameters, $\{p_i\}$, are chosen according to the CIP, is robust against a perturbation to the choice of the qubit-bath interaction parameter. Note here that the crucial feature of $\{p_i\}$, according to the CIP, is the specific ratios of p_1, p_2, and p_3 to each other. Therefore, to investigate the robustness, we deviate the values of $\{p_i\}$ from CIP as $p_i \to p_i + \epsilon_i$, where $\epsilon_i = u_i \times 10^{-v_i} \ll p_i$, $\{u_i\}$ and $\{v_i\}$, $i = 1, 2, 3$, being positive real numbers, and find the answer to the above question to be in the affirmative. Keeping the values of x and y to be the same as in Fig. 4.1(a), the broad qualitative features of the transient refrigeration without the steady-state refrigeration is found unaltered with small perturbations in the form of non-zero values of $\{u_i\}$ and $\{v_i\}$, although the quantitative aspects, such as the values of T_{min} and t_{min}, change. This is depicted in Fig. 4.1(b), where we plot the variation of $T_c(t)$ as a function of t for two sets of values of $\{v_i\}$, while keeping $\{u_i = 1\}$.

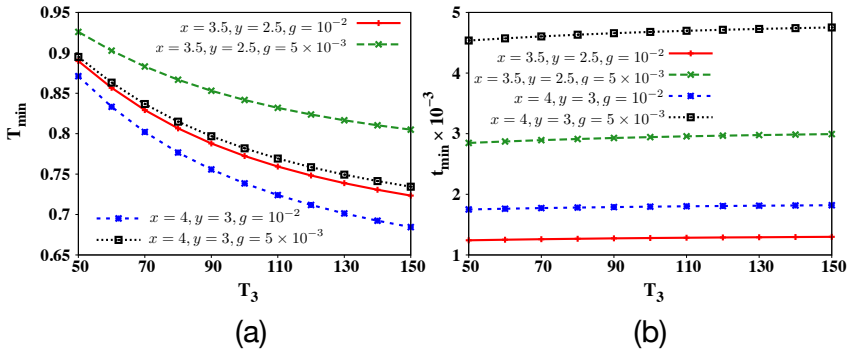

Figure 4.3: Effect of temperature of the hot bath in the reset model. We plot the variations of (a) T_{min} and (b) t_{min} as functions of T_3 for different values of x and y, given by $(x, y) = (3.5, 2.5)$ and $(4, 3)$, and for different values of g, given by $g = 10^{-2}, 5 \times 10^{-3}$. The values of (x, y) are chosen from the region marked "**R**" in Fig. 4.2. All quantities plotted are dimensionless. Keeping T_3 and T_1 fixed at the values investigated, increase of T_2 results in an increase of the lowest temperature that can be achieved by the cold qubit in the transient regime.

Next, we establish that there exists substantial regions in the space of $\{p_i\}$, where TC is the only option to obtain refrigeration. In Fig. 4.2, we plot (a) T_1^s, (b) $T_{\rm min}$, and (c) $t_{\rm min}$ as functions of x and y for fixed values of g. Here,

$$T_{min} = \min_t T_c(t), \tag{4.9}$$

and t_{min} is the time at which this minimization occurs. To perform the minimization as well as for obtaining a typical dynamics profile, we always focus on the range $0 \leq t \leq 10^5$. In this section, and in all the subsequent discussions, we consider $t = 10^5$ to be large time. In all the graphs shown in this paper, steady state of the system is achieved for $t < 10^5$. We find that over a large set of points considered on the (x, y)-plane, bounded by $2 \leq x \leq 4$ and $0 \leq y \leq 3$, the temperature of the cold qubit almost reaches the steady state temperature at or before $t = 10^5$. The lines on the graph in Fig. 4.2(a) refer to the lines corresponding to fixed values of T_1^s, the steady state temperature of the cold qubit (qubit 1). We observe that there exist regions on the (x, y)-plane (the region above the line corresponding to $T_1^s = 0.99$), where $T_1^s \approx 1$, implying a negligible or no steady state cooling, and so in these regions, transient cooling is the only plausible alternative.

Indeed, we find that in these regions, T_{min} can have a significantly low value compared to the initial temperature of the cold qubit, T_1. This situation is "rich" in the first quadrant of the region considered over the (x, y)-plane, which we mark by "**R**", and enclose by the dotted lines. Here, therefore, we find a large number of instances where the system provides a refrigeration that is necessarily transient. Qualitatively similar results are found for different values of g. Note here that $T_1^s \leq 1$ over the entire region of the (x, y)-plane considered, which implies that no steady state heating has taken place in this parameter space. We will see in the next subsection that this is not the case when a different thermal bath is considered.

It is evident from Figs. 4.1 and 4.2 that better cooling is achieved when g is high, x is high, and y is low. Lower T_{min} with increase in g is expected as the cooling occurs for the three-body interaction with specific initial bias and higher value of the interaction strength provides better cooling. Note also that as the transient cooling occurs in single-shot scenario, the T_{min} is achieved in the initial stage of the dynamics, which is mostly dominated by the unitary interaction. Hence, the transient cooling in this regime also gets better when the bath couplings are small. As is seen from Fig. 4.2, for a fixed value of y, T_{min} is lower if x is higher, as $\{p_i\}$ varies linearly with 10^{-x}, whereas for a fixed value x, T_{min} is lower if y is lower, as p_3 is the strongest bath coupling parameter and it varies linearly with 10^{-y}.

Note here that the time, t_{min}, required to attain the minimum temperature during transient refrigeration, is a complex function of the system as well as the qubit-bath interaction parameters. In the standard models of thermalization for the three-qubit quantum refrigerator used in this paper, high values of the qubit-bath interaction parameters tend to keep the qubits in thermal equilibrium with their respective heat baths, while the inter-qubit interaction strength, g, drives them away from equilibrium. The time of optimal transient cooling is inversely proportional to the interaction strength g, but it occurs, in the reset model, much later than the half time period π/g, as the bath coupling strengths exceed the

interaction strength g (see [145, 147]).

Effect of system parameters. It is interesting to ask how the performance of the refrigerator is modulated by the parameters of the system. To investigate this, we choose the temperature of the hottest bath, i.e., T_3, as the tuning parameter, and study the variation of the minimum temperature, T_{min}, achieved during transient refrigeration, against T_3, when the choice of the qubit-bath interaction parameters do not allow steady-state refrigeration. For this purpose, we choose the values of $\{p_i\}$ according to the CIP, and restrict ourselves to the region marked by "**R**" in Fig. 4.2. Fig. 4.3 depicts the variations of T_{min} and t_{min} against T_3 for different sets of values of $\{p_i\}$, governed by different sets of values of x and y. The minimum temperature achieved by the transient refrigeration, without the steady-state refrigeration, is found to decrease monotonically with increasing values of T_3. On the other hand, the corresponding values of t_{min} is found to increase very slowly with T_3. This proves the transient refrigerator to be advantageous, in the sense that for a fixed set of qubit-bath interaction parameters chosen according to the CIP, a lower temperature can be achieved at effectively the same time, by increasing the temperature of the hot bath. However, we point out here that T_{min} can not be indefinitely lowered with increasing T_3. For sufficiently high value of T_3, T_{min} attains a saturation at a minimum value. Also note that the relative positions of the graphs of T_{min} as well as t_{min} corresponding to different values of (x, y) and g, clearly suggests that the variations of T_{min} as well as t_{min} are non-monotonic with respect to the qubit-bath interaction parameters and the qubit-qubit interaction parameter. This is also supported by the data shown in Fig. 4.2.

Fast and steady cooling. Let us now study a situation where we relax the condition $T_1^s \approx T_1$. We are now interested to change CIP in such a way that an occurrence of SSC takes place very fast, and the steady state temperature, T_1^s, is the minimal temperature. Such phenomenon emerges by interchanging κ_1 and κ_2, which, following Eq. (4.8), leads to $\kappa_1 \leq \kappa_2$. As an example, we consider the case of $x = 2.5$ and $y = 1$, such that $p_1 = 10^{-2.5}$, $p_2 = 10^{-3.5}$, and $p_3 = 10^{-1.5}$, for which the variation of $T_c(t)$ is depicted in Fig.

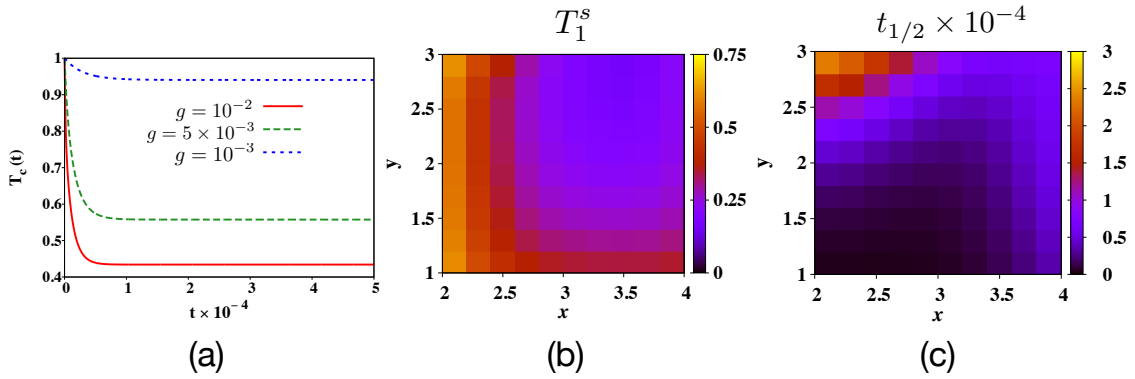

Figure 4.4: Fast and steady cooling in the reset model. We plot (a) the variation of $T_c(t)$ versus t. We choose $x = 2.5$, $y = 1$, and $g = 10^{-3}$, 5×10^{-3}, and 10^{-2}. The occurrence of the phenomena in substantial region in the qubit-bath interaction parameter space is demonstrated by plotting the variations of (b) T_1^s and (c) $t_{1/2}$ with x and y for $g = 10^{-2}$. All quantities are dimensionless.

4.4(a) for $g = 10^{-3}$, 5×10^{-3}, and 10^{-2}. The temperature of the cold qubit decreases rapidly with time, and becomes steady at a temperature much lower than its initial temperature, given by $\min_t T_c(t)$. The value of T_1^s is found to increase with decreasing g. Moreover, note that for these parameter values, unlike previous studies in [143], $T_c(t)$ does not show any oscillation with t.

Let us introduce the quantity $\delta_c = T_1 - T_1^s$, which quantifies the maximum cooling that is obtained in the scenario. We define the "half-time", $t_{1/2}$, as the time at which $T_c(t) = T_1 - \frac{\delta_c}{2}$. In the case of the damped coherence dynamics, the half-time provides a measure of how fast the temperature of the cold qubit approaches its minimum value, which is the steady state temperature. The lower the value of $t_{1/2}$, the faster is the approach of the cold qubit to its steady state. However, even when the coherence dynamics is not damped, a lower value of $t_{1/2}$ indicates that there is a possibility of significantly fast cooling of the cold qubit before it reaches its steady state.

As in the previous case, we investigate whether this phenomenon occurs in a considerable region of the parameter space. In order to do so, we focus on the region $2 \leq x \leq 4$ and $1 \leq y \leq 3$ over the (x, y)-plane. Fig. 4.4(b)-(c) depicts the variations of (b) T_1^s, and (c) $t_{1/2}$ as functions of x and y for $g = 10^{-2}$. Note that in contrast to the previous case of

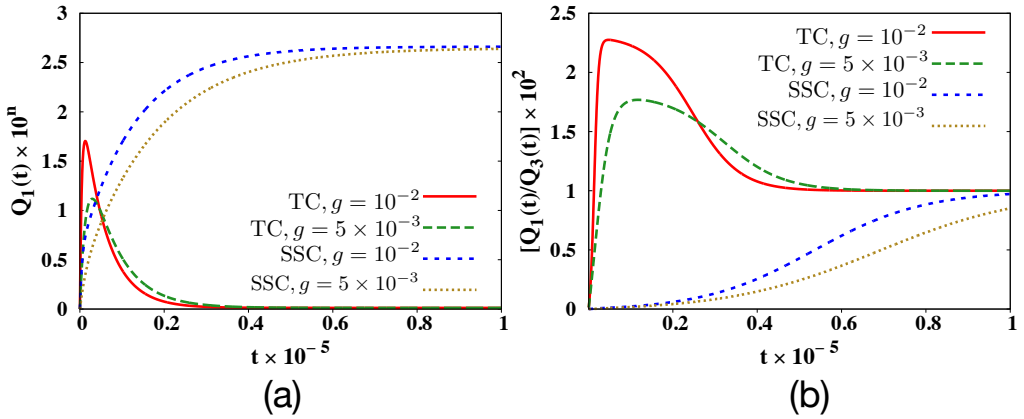

Figure 4.5: Performance of the necessarily transient refrigerator in the reset model. (a) Variations of the cooling power are exhibited as functions of time in case of a necessarily-transient refrigerator ($p_1 = 10^{-3.5}, p_2 = 10^{-6}, p_3 = 10^{-1}$), and in case of the occurrence of fast and steady cooling ($p_1 = 10^{-6}, p_2 = 10^{-3.5}, p_3 = 10^{-1}$), where $(x, y) = (3.5, 2.5)$. The exponent in the multiplicative factor to Q_1 is $n = 5$ in the former case, and $n = 7$ in the latter. (b) Plot of variations of the ratio of heat currents agianst time, where all the parameter values relevant to the dynamics are the same as in (a), except for an interchange between p_1 and p_2. All quantities are dimensionless.

transient refrigeration, substantial steady state cooling takes place in the present situation, as can be clearly understood from the range of the values of T_1^s.

Note. For the purpose of demonstration, we plot in Fig. 4.1 only those dynamics profiles where no initial oscillation of $T_c(t)$ takes place. However, initial oscillation of $T_c(t)$ is indeed possible from the CIP, depending on the values of g and $\{p_i\}$. In most of the cases corresponding to CIP, damped coherence dynamics is observed when one approaches steady state cooling (eg. Fig. 4.4), which implies a faster cooling without precise time control.

Cooling power and ratio of heat currents:

The rate of heat flow between qubit i ($i \in \{1, 2, 3\}$) and the corresponding bath at any time t, called *heat current*, is given by $Q_i(t) = \mathrm{Tr}[H_i p_i(\tau_i \otimes \mathrm{Tr}_i \rho(t) - \rho(t))]$, H_i being the local Hamiltonian of the ith qubit. The coefficient of performance (COP) of the three-qubit absorption refrigerator [1, 131, 139, 144] is $\varepsilon = Q_1^S / Q_3^S$, where Q_i^S is the heat current of qubit i in steady state ρ^S, given by $Q_i = \mathrm{Tr}[H_i p_i(\tau_i \otimes \mathrm{Tr}_i \rho^S - \rho^S)]$. Cooling of qubit 1

is indicated by a flow of heat from the bath to the qubit, which is reflected by a positive value of $Q_1(t)$. The time-behaviour of $Q_1(t)$, also referred to as *cooling power*, has been demonstrated in Fig. 4.5(a). We study how the ratio of the heat currents approach the value of COP at steady state. Fig. 4.5(b) shows this ratio as functions of time with different values of g, for both the cases when TC without SSC occurs, or SSC takes place with transient temperature monotonically decreasing to the steady-state temperature. Please note that this ratio can have a higher value at transient times compared to the steady state value. But if we want to achieve the higher transient value, we have to introduce an external device to switch off the inter-qubit interaction at that point of time. The work thus performed by the external device should be taken into account while defining COP in transient regime. However, we do not take into account this work done in any of our numerical calculations, hence COP is only well-defined for steady state of refrigerator.

4.1.2 Thermalization by memoryless qubit-bath interaction

Let us now move to a more realistic scenario, under the standard Born-Markov assumption of a memoryless system-bath interaction. Our aim is again to find out a range of parameters which can be tuned in such a way that the refrigeration occurs only in the transient regime. The dynamics of this model is governed by a quantum master equation of the Lindblad form, given in Eq. (4.4). The difference of this model from the previous one lies in the choice of the bath. In this case, each qubit is coupled to a bath constituted of an infinite set of harmonic oscillators having a broad range of frequencies, ω. The total Hamiltonian of the bath is given by $\tilde{H}_b = \sum_{i=1}^{3} \hbar\nu_{i,k} b_{i,k}^{\dagger} b_{i,k}$, where we assume the baths to be spatially well separated to neglect any interaction between them. Here, $\nu_{i,k}$ is the frequency of the mode k of the bath i, and the b's are the bosonic mode operators. The interaction Hamiltonian between the qubits and the baths is given by $\tilde{H}_{sb} = \sum_{i=1}^{3} \mathcal{A}_i \otimes \mathcal{X}_i$, where $\mathcal{A}_i = \sigma_i^x$ are the Lindblad operators responsible for transitions between different eigenstates of the fully-coupled Hamiltonian $\tilde{H}_{loc} + \tilde{H}_{int}$, and $\mathcal{X}_i = \sum_{i=1}^{3} (\eta_{i,k} b_{i,k} + \eta_{i,k}^{*} b_{i,k}^{\dagger})$

are the collective bath co-ordinates. Here, the subscript "sb" stands for "system-bath", and the strength of the qubit-bath couplings are denoted by $\eta_{i,k}$. The Hamiltonian describing the system consisting of the three qubits and their respective baths is then given by $\tilde{H}_{tot} = \tilde{H}_{loc} + \tilde{H}_{int} + \tilde{H}_b + \tilde{H}_{sb}$. We assume that the spectral function corresponding to the bath i is of the form of an Ohmic spectral function, given by $\tilde{J}_i(\omega) = \alpha_i \omega \exp(-\omega/\Omega)$ where α_i is the dimension-less coupling strength defining the qubit-bath coupling, and Ω is the "cut-off frequency", such that the memory time of the baths $\sim \Omega^{-1}$. Since we are interested in the Markovian dynamics, Ω must be much larger than a typical frequency ω, while $\alpha_i << 1$ [145].

We now consider the specific case of this thermalization model, where the dissipation rates are much smaller than the coupling strength, g. Following [145], one can derive the Markovian master equation for the three-qubit system in this model described above. Here, the operation Φ in the master equation is given by

$$\Phi(\rho) = \sum_{i,\omega} \tilde{\gamma}_i(\omega) \varphi_i^{\omega}(\rho), \tag{4.10}$$

where $\{\tilde{\gamma}_i(\omega)\}$ represents the incoherent transition rates between the eigenstates of the Hamiltonian $\tilde{H}_{loc} + \tilde{H}_{int}$. In terms of the spectral functions of each bath, $\tilde{\gamma}_i(\omega)$ can be obtained as [145]

$$\tilde{\gamma}_i(\omega) = \begin{cases} \tilde{J}_i(\omega)\{1 + f(\omega, \tilde{\beta}_i)\}, & (\omega > 0) \\ \tilde{J}_i(|\omega|) f(|\omega|, \tilde{\beta}_i), & (\omega < 0) \end{cases} \tag{4.11}$$

where $f(\omega, \tilde{\beta}) = \{\exp(\hbar\tilde{\beta}\omega) - 1\}^{-1}$ represents the Bose-Einstein distribution. The operation φ_i^{ω} in Eq. (4.10) is given by [145]

$$\varphi_i^{\omega}(\rho) = \mathcal{L}_i^{\omega} \rho \mathcal{L}_i^{\omega\dagger} - \frac{1}{2}\{\mathcal{L}_i^{\omega\dagger} \mathcal{L}_i^{\omega}, \rho\}$$

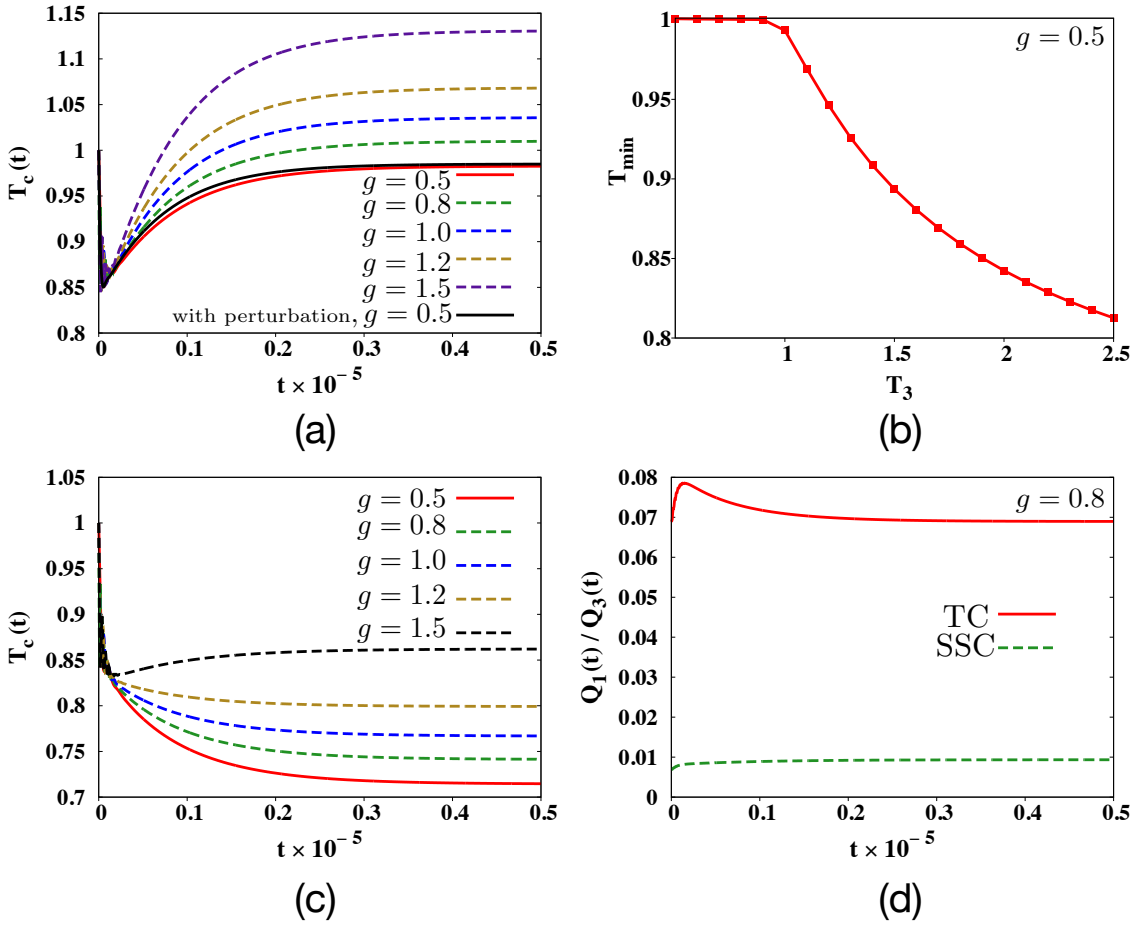

Figure 4.6: Necessarily transient refrigerator for thermalization with collections of harmonic oscillators as local heat baths. (a) We plot $T_c(t)$ against t, choosing $x = 4$ and $y = 1$, and $\{\alpha_i; i = 1, 2, 3\}$ as in Eq. (4.8), for different values of g. (b) The variation of $T_{\min}$ with T_3 for the case when $g = 0.5$. All other relevant parameters are as in panel (a). (c) The occurrence of fast and steady cooling, with and without transient cooling, is depicted in this panel for different values of g. We have interchanged α_1 and α_2, while keeping the value of (x, y) to be the same as in (a). (d) Variation of the ratio of heat currents as a function of time for $g = 0.8$ in two different scenarios: one where TC without SSC takes place (as shown in (a), with the relevant parameters unchanged), and the other one where fast SSC takes place without TC (as shown in (c), with the relevant parameters unchanged). The value of the coefficient is considerably larger in the former case for all values of t, compared to the latter. All quantities are dimensionless.

where the Lindblad operators, $\{\mathcal{L}_i^{\omega}\}$, have the explicit forms given by

$$\begin{aligned}
\mathcal{L}_1^{E_1} &= |111\rangle\langle 011| + |100\rangle\langle 000|, \\
\mathcal{L}_1^{(E_1+g)} &= (|+\rangle\langle 001| - |110\rangle\langle -|)/\sqrt{2}, \\
\mathcal{L}_1^{(E_1-g)} &= (|110\rangle\langle +| + |-\rangle\langle 001|)/\sqrt{2}, \\
\mathcal{L}_2^{E_2} &= |110\rangle\langle 100| + |011\rangle\langle 001|, \\
\mathcal{L}_2^{(E_2+g)} &= (|+\rangle\langle 000| + |111\rangle\langle -|)/\sqrt{2}, \\
\mathcal{L}_2^{(E_2-g)} &= (|111\rangle\langle +| - |-\rangle\langle 000|)/\sqrt{2}, \\
\mathcal{L}_3^{E_3} &= |111\rangle\langle 110| + |001\rangle\langle 000|, \\
\mathcal{L}_3^{(E_3+g)} &= (|+\rangle\langle 100| - |011\rangle\langle -|)/\sqrt{2}, \\
\mathcal{L}_3^{(E_3-g)} &= (|011\rangle\langle +| + |-\rangle\langle 100|)/\sqrt{2},
\end{aligned} \tag{4.12}$$

with $|\pm\rangle = (|010\rangle \pm |101\rangle)/\sqrt{2}$. Going to the dimensionless form, we see that the second term on the right-hand-side of Eq. (4.5) can be written as

$$\frac{\hbar}{k}\Phi(\rho) = \sum_{i,\omega} \gamma_i(\omega)\varphi_i^{\omega}(\rho), \tag{4.13}$$

where $\gamma_i(\omega) = \frac{\hbar}{k}\gamma_i(\omega)$, and $J(\omega) = \frac{\hbar}{k}\tilde{J}(\omega)$. The transitions between a pair of eigenstates of $H_{loc} + H_{int}$, having an energy difference corresponding to ω, is governed by the operator $\mathcal{L}_i^{\omega}$, while a similar operation corresponding to an energy difference of $-\omega$ is represented by $\mathcal{L}_i^{-\omega} = \mathcal{L}_i^{\omega\dagger}$. Note here that for the rotating wave approximation to be a valid one, in the present case, one has to consider a parameter space where a typical time-scale of the system is much smaller than the dissipation time, implying $\min\{E_i, g\} \gg \max\{\gamma_i\}$ [145].

Refrigeration in a necessarily transient regime. To obtain cooling only in the transient regime, CIP plays an important role to tune the qubit-bath interaction parameters, $\{\alpha_i\}$, like in the previous case. For the purpose of demonstration, we choose $x = 4$ and $y = 1$. We set the other system parameters as $E_3 = 1$, and $T_3 = 2$, and E_2 is fixed by the equation

$E_2 = E_1 + E_3$, with $E_1 = 1$ and $T_1 = 1$. The corresponding variation of $T_c(t)$ as a function of t is depicted in Fig. 4.6(a) for different values of g in the range $0.5 \leq g \leq 1.5$. It is clear from the figure that for a low value of g, the steady state temperature of the cold qubit may be lower than its initial temperature, T_1. However, with increasing g, the value of T_1^s increases, and eventually crosses T_1, thereby moving over to a region where a *steady state heating* of the cold qubit takes place. In this scenario, the necessity of a transient refrigeration of the cold qubit is pressing, and is obtainable at a sufficiently low time, as shown in the figure. Moreover, one should note that in the previous model, we were unable to find any range of parameters where $T_1^s > T_1$, which is observed in this model.

A word on the occurrence of the steady state heating in the case of the harmonic oscillator bath model is in order here. Note that the unitary dynamics swaps the populations of the states $|101\rangle$ and $|010\rangle$. Heating of qubit 1 implies increasing the population of the state $|010\rangle$. However, the initial condition of the dynamics corresponding to the three-qubit absorption refrigerator involves a bias where the population of the state $|010\rangle$ is higher than the population of the state $|101\rangle$. Therefore, the heating of the qubit 1 is not possible by the interaction unitary itself. But due to the strong coupling here, transitions occur between the eigenstates of the Hamiltonian $H_{ref} = H_{loc} + H_{int}$. It can be seen from the Lindbladian operators $\{L_i^w\}$, that cooling as well as heating is possible due to the transitions in the dissipative dynamics. The net result, i.e., whether heating or cooling will actually occur, depends on the transition rates. Steady state heating for large interactions indicates the dominance of the transitions in large time. In contrast, in the case of the reset model, as the thermalization of the qubits brings them to their corresponding initial thermal states, the temperature of the cold qubit cannot be increased due to thermalization. Hence, no steady state heating is observed for the reset model.

Robustness. We test the robustness of the CIP for a necessarily transient cooling to take place, by considering small perturbations to the CIP. We take the same form of perturbations as discussed in Sec. 4.1.1, and find that similar to the case of the reset model,

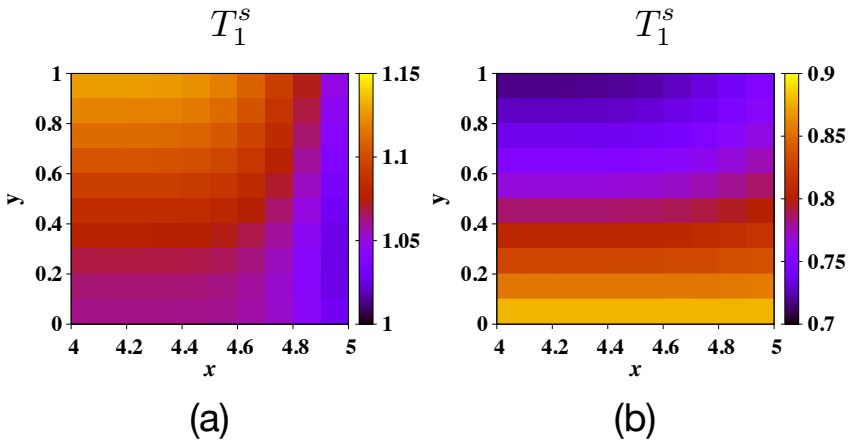

Figure 4.7: System characteristics of the refrigerator modeled in Sec. 4.1.2. (a) We present projection plot of T_1^s as functions of x and y. Here, $g = 1.5$. (b) Variation of T_1^s with x and y where fast and steady cooling take place instead of TC without SSC. Here, we choose $g = 0.5$. All quantities plotted are dimensionless.

for small perturbations, the phenomena of TC without SSC remains unchanged, although quantitative changes may take place to the minimum achievable temperature, or the time when the minimum temperature is achieved.

Fast and steady cooling. We now mention the case where the possibility of fast and steady cooling exists with the low values of g. For example, consider the plots of $T_c(t)$ as functions of t for different values of g in the range $0.5 \leq g \leq 1.5$, as presented in Fig. 4.6(c). Here also, we consider $\alpha_1 = 10^{-(x+y)}$, $\alpha_2 = 10^{-x}$ and $\alpha_3 = 10^{-(x+y)}$ to generate such dynamics, and we choose $x = 4$ and $y = 1$ for the purpose of demonstration. All the other system parameters are set to the same values as in the case of the transient refrigeration. We find that for low values of g, the cooling occurs considerably fast, and the steady state value is the coldest temperature attainable by the cold qubit, while for high values of g, the SSC can take place simultaneously with a TC, as is clear from Fig. 4.6(c).

Variation with T_3. Similar to that for the reset model, here also we check the variation of the minimum temperature attained by the refrigerator as a function of the temperature of the hot bath. We find that with increase of T_3, T_{min} at first remains constant at $T_{min} = T_1$, and then on further increase of T_3, it monotonically decreases. This behaviour is demonstrated in Fig. 4.6(b). The variation of t_{min} with T_3 is a slow one. This implies

that one has to increase the temperature of the hot qubit above a critical value to obtain TC. Besides, it shows that the under the present model of qubit-bath interaction also, transient refrigeration without steady-state refrigeration can be made advantageous with an increase in the temperature of the hot bath. Also, as in the case of the reset model, the CIP is robust against small perturbations with respect to the display of the phenomena of transient refrigeration without the steady state refrigeration.

Performance. Similar to the case of the reset model, we study the cooling power and ratio of heat currents in the case of the present model also. Here, the heat current from qubit i ($i \in \{1,2,3\}$) to the corresponding bath [139], at time t, is given by $\mathcal{Q}_i(t) = \mathrm{Tr}[\tilde{H}_{ref} \sum_\omega \tilde{\gamma}_i(\omega)\varphi_i^\omega(\rho)]$, and the COP is $\epsilon = \frac{\mathcal{Q}_1}{\mathcal{Q}_3}$. Here, $\tilde{H}_{ref} = \tilde{H}_{loc} + \tilde{H}_{int}$. Note here an apparent difference between the definitions of the heat currents here and in the case of the reset model. These are however equivalent, considering that the reset model assumes the interaction strength g to be small. In Fig. 4.6(d), the variation of the cooling power corresponding to the refrigerator in two different scenarios is depicted for $g = 0.8$. The first scenario is the one where TC without SSC takes place, while in the second, SSC occurs with or without TC.

Frozen minimum temperature. Let us now systematically investigate the range of (x, y) values where transient cooling is required for the three-qubit system to act as a refrigerator. We choose the region defined by $4 \leq x \leq 5$, and $0 \leq y \leq 1$, which is justified by the validity of the quantum master equation and the form of the operator Φ (Eq. (4.10)). In Fig. 4.7(a), the variations of T_1^s as a functions of x and y are presented for a fixed value of $g = 1.5$. It is clear from Fig. 4.7(a) that in the entire region of the (x, y)-plane considered, a steady state heating takes place, and transient cooling is the only option to use the three-qubit system as a refrigerator for the cold qubit. Similar to that in the reset model, we again determine the value of T_{min} by performing a scan over the dynamics profiles up to $t = 5 \times 10^4$. We find that for all the points in the region considered over the (x, y)-plane, the cold qubit reaches its minimum temperature very fast. This time of reaching the min-

imum temperature is negligible compared to the typical large times required by the cold qubit to attain its steady states. Curiously, over the entire region considered, the value of T_{min} is effectively *frozen* at a value $T_{min} = 0.842$, with the variation occuring only in the fourth decimal place. This provides one the liberty to choose an appropriate set of values for x and y, when the transient refrigeration is implemented in the laboratory.

Note here that in contrast with the reset model discussed earlier, the present model is operating in the strong coupling regime, where the interaction g is much larger than the qubit-bath coupling strengths. Here, the initial dynamics is dictated by the coherent dynamics and the temperature of the cold qubit oscillates with time period π/g. The minimum temperature here is achieved in the first half cycle, i.e., at $\pi/2g$, and the minimum temperature is independent of the bath couplings.

To investigate whether a substantial region in the parameter space can be found where fast SSC takes place, we focus on the same region over the (x, y)-plane as discussed in the case of transient cooling, bounded by $4 \leq x \leq 5$, and $0 \leq y \leq 1$. We find that such a cooling phenomenon is present in a considerable part of our region of interest on the (x, y)-plane, as also obtained in the case of the reset model in Fig. 4.4(b). The variations of T_1^s, as a function of x and y, is presented in Fig. 4.7(b), which also gives further basis to believe in the generic nature of the observation of the previous model. With increasing g, the value of the steady state temperature increases (as also shown in Fig. 4.6(c)), and after a critical value, the dynamics pattern changes in such a way that the steady state temperature is no longer the minimum temperature of the cold qubit.

4.2 Quantum correlations of the necessarily transient refrigerator

We now investigate the properties of bipartite and multipartite correlations in the parameter space of the models discussed in this paper.

4.2.1 Bipartite quantum correlations

We start with the bipartite quantum correlations, as measured by logarithmic negativity (LN) [14, 15, 25, 27, 28, 152], denoted by $\mathcal{L}$, from the entanglement-separability domain, and quantum discord (QD) [38, 40, 153–157], denoted by $\mathcal{D}$, from the information-theoretic domain. Since the initial state of the dynamics, governed by the master equation given in Eq. (4.4), is a product state, both LN and QD are zero in all bipartitions for the three-qubit state at $t = 0$. As the system evolves in time, one expects generation of bipartite quantum correlations in different bipartitions of the three-qubit system at $t > 0$. This is indeed the case when LN in the case of the reset model is considered. For example, we consider the parameter values $x = 3.5$, $y = 2.5$, and plot LN against t in the bipartition $1 : 23$ in Fig. 4.8(a), keeping $g = 10^{-2}$. All the other system parameters are kept at the values as in Fig. 4.2. We find that LN increases at first, reaches a maximum, and then decreases sharply to be zero at $t \sim 200$, which is low compared to the large time scale ($\sim 10^5$) considered in this paper. Let us denote the maximum possible value of LN in $0 \leq t \leq 500$ for the bipartition $1 : 23$ by $\mathcal{L}^m_{1:23}$. In the inset of Fig. 4.8(a), we plot $\mathcal{L}^m_{1:23}$ as a function of x and y. The maximum value of $\mathcal{L}^m_{1:23}$ that is attained in the (x, y)-plane considered in Fig. 4.8(a) is ~ 0.016, which is considerably low. Similar qualitative features are found in the case of $\mathcal{L}_{2:13}$ and $\mathcal{L}_{3:12}$ also.

Note that in major portions of (x, y)-plane considered in Fig. 4.8(a), the values of $\mathcal{L}^m_{1:23}$ are low – a feature shared qualitatively by $\mathcal{L}^m_{2:13}$ and $\mathcal{L}^m_{3:12}$. Comparing $\mathcal{L}^m_{1:23}$ with

T_{min} (comparison between the region "**R**" marked in Fig. 4.2(b), and inset of Fig. 4.8(a)), we find that $\mathcal{L}^m_{1:23}$ possesses higher values whenever T_{min} is low in the region "**R**". The value of $\mathcal{L}^m$, in all bipartitions, decreases with decreasing g.

Fig. 4.8(b) depicts the variation of QD, $\mathcal{D}_{1:23}$, in the bipartition $1:23$ in the case of the reset model, with all the parameters being identical to that used in the case of LN. We find that $\mathcal{D}_{1:23}$ increases with t at first, attains a maximum, and then decreases slowly with increasing t. The slow decay of QD with increasing t is in contrast with the sharp decrease of LN. Similar to LN, in the present case also, one can define $\mathcal{D}^m_{1:23}$ corresponding to the bipartition, $1:23$. In the inset of Fig. 4.8(b), $\mathcal{D}^m_{1:23}$ is plotted as a function of x and y in the region "**R**", showing a qualitatively similar variation of $\mathcal{D}^m_{1:23}$ to that of $\mathcal{L}^m_{1:23}$. The maximum value of $\mathcal{D}^m_{1:23}$, found in the region "**R**", is higher than that corresponding to LN. Similar to the case of LN, $\mathcal{D}^m_{1:23}$ has higher values whenever T_{min} acquires comparatively lower values in the region "**R**, in the case of the reset model. Therefore, it seems that for the reset model, a low value of temperature of the cold qubit in the transient regime with the parameter values considered in this paper is related to high quantum correlations generated in the bipartition $1:23$. The qualitative behavior of QD in the other two bipartitions are similar to that in the bipartition $1:23$.

In the more realistic model discussed in Sec. 4.1.2, for all sets of parameters values, (x, y), considered in Fig. 4.7, no bipartite entanglement is generated in any of the bipartitions for $t > 0$. However, QD is found to be generated in all the bipartitions at $t > 0$ for the collection of values of (x, y) chosen in Fig. 4.7. Fig. 4.8(c) depicts the variation of $\mathcal{D}_{1:23}$ as a function of t, with $x = 4$, $y = 1$, and $g = 1.5$. All the other parameters are set at values as in Fig. 4.7. The dynamics of QD is found to be oscillatory at first. The oscillation dies out as t increases, and the system approaches towards its steady state. The maximum value of QD is reached during the oscillatory part of the dynamics. The variation of $\mathcal{D}^m_{1:23}$, as a function of x and y, is represented in the inset of Fig. 4.8(c), where $g = 1.5$, and similar range of (x, y) values, as presented in Fig. 4.7, is chosen. The other

parameter values are kept fixed at values as in Fig. 4.7. We observe that high values of $\mathcal{D}^m_{1:23}$ are found when x is low, and y is high, which is in contrast to the findings in the reset model, where both $\mathcal{L}^m_{1:23}$ and $\mathcal{D}^m_{1:23}$ are high when x is high and y is low.

4.2.2 Multipartite correlations

Next, we consider the properties of multiparty correlations in the time-evolved state of the reset model and the realistic model discussed in this paper. As a measure of the tripartite total correlation, we consider the tripartite total mutual information, given by $\mathcal{I}_{tot}$ [158, 159], and plot its variation against t in he case of the reset model (Fig. 4.8(d)) and the realistic model (Fig. 4.8(e)). The values of the qubit-bath interaction parameters are set to values similar to those in Fig. 4.1 for the reset model, and in Fig. 4.6 for the realistic model. We find that in the case of the reset model, the value of $\mathcal{I}_{tot}$ increases with t at first, reaches a maximum, and then decreases to attain a saturation value close to zero at high t. This feature remains unaltered in the entire region **R**, marked in Fig. 4.2. Let us denote by $\mathcal{I}^m_{tot}$, the maximum value of $\mathcal{I}_{tot}$ that is attained during the evolution of the system under the reset model, for a fixed set of values of x and y. In the inset of Fig. 4.8(d), we plot the variation of $\mathcal{I}^m_{tot}$ as a function of x and y in the region **R**. Note that similar to the bipartite correlations discussed in Sec. 4.2.1, the values of $\mathcal{I}^m_{tot}$ is high when x is high and y is low.

On the other hand, in the case of the realistic model, a typical evolution of $\mathcal{I}_{tot}$ involves an initial oscillation, and then a saturation at a non-zero value for high t, as depicted in Fig. 4.8(e). Similar to the previous case, here also we consider the variation of $\mathcal{I}^m_{tot}$ as function of x and y in the region **R** marked in Fig. 4.7. Although in most of the regions on the (x, y)-plane, the value of $\mathcal{I}^m_{tot}$ is low, which is in agreement with the findings in case of the reset model, comparatively high values of $\mathcal{I}^m_{tot}$ are found when both x and y are low, in contrast to what is found for the reset model.

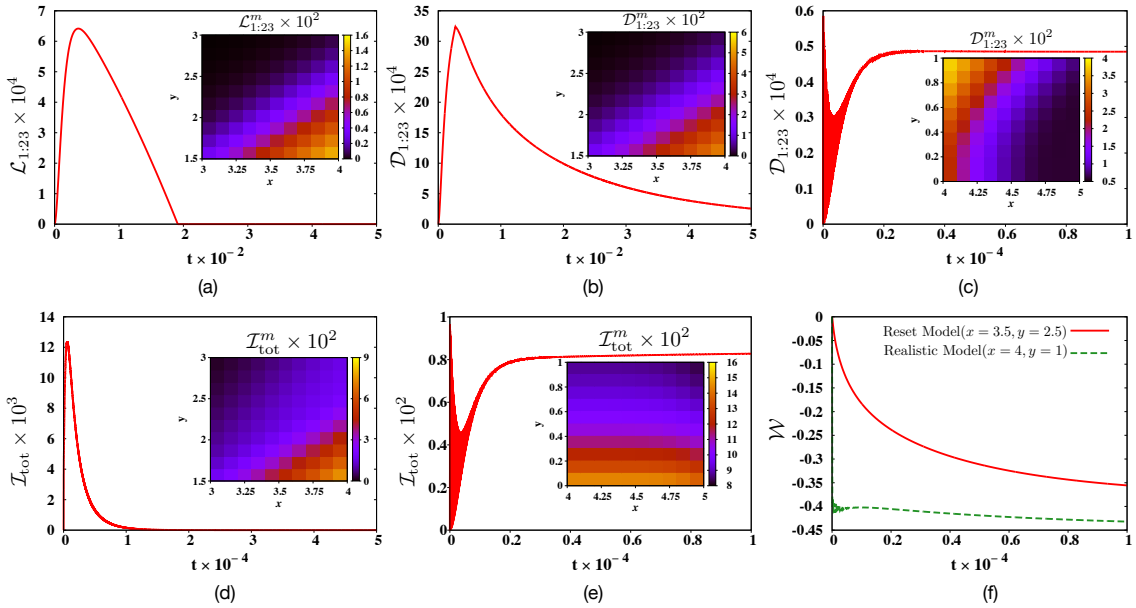

Figure 4.8: Bipartite and multipartite correlations in necessarily transient refrigerator. Variations of (a) LN for the reset model, (b) QD for reset model, and (c) QD for the realistic model in the bipartition $1:23$, as functions of t are depicted in the top row of panels. For demonstration, we choose $x = 3.5$, $y = 2.5$, $g = 10^{-2}$ for the reset model, and $x = 4$, $y = 1$, $g = 0.5$ for the realistic model, while all the other parameters are fixed at the same values as in Fig. 4.2 and Fig. 4.7 for the reset model and the realistic model, respectively. In the insets of (a)-(c), variations of (a) $\mathcal{L}^m_{1:23}$ for the reset model, (b) $\mathcal{D}^m_{1:23}$ for the reset model, and (c) $\mathcal{D}^m_{1:23}$ for the realistic model, as functions of x and y are exhibited. We have chosen $g = 10^{-2}$ and $g = 1.5$ for the reset and the realistic model, respectively, for demonstration. All the other parameters are fixed at the same values as in Figs. 4.2 and 4.7. In the bottom row of panels, we show variation of the tripartite total mutual information, $\mathcal{I}_{tot}$, for (d) the reset model and (e) for the realistic model. We also depict the behavior of (f) the genuine tripartite concurrence detector, $\mathcal{W}$, for the reset and the realistic models, as functions of t. The values of different parameters chosen for demonstration are similar to those in (a), (b), and (c). In the insets of (d) and (e), variations of $\mathcal{I}^m_{tot}$ for (d) the reset model and (e) the realistic model, as functions of x and y are shown. All the other parameters are fixed at the same values as in the insets of (a), (b), and (c). All the quantities plotted in all the panels are dimensionless.

We now discuss the generation of multiparty quantum correlations in the models discussed in this paper. Note here that there are only a few *computable* measures of multiparty quantum correlations, in both entanglement-separability and information-theoretic domains. A quantification of multipartite quantum correlations, in terms of bipartite quantum correlations, can be obtained in terms of the monogamy scores, given by δ_Q [160, 161], corresponding to the chosen bipartite quantum correlation measures. However, since no coherence is generated during the dynamics in the present scenario, all the two-qubit reduced density matrices obtained from the three-qubit time-evolved state, under both the models, are diagonal in the computational (product) basis. This implies that in a certain bipartition, say, $1 : 23$, the values of $\delta_{\mathcal{L}}$ and $\delta_{\mathcal{D}}$ are given by $\mathcal{L}_{1:23}$ and $\mathcal{D}_{1:23}$, respectively, the features of which have been discussed in Sec. 4.2.1. To investigate whether any genuine tripartite entanglement is generated during the dynamics, we focus on an entanglement witness, $\mathcal{W}$ [162, 163], which indicates the presence of genuine tripartite concurrence [164, 165] when $\mathcal{W} > 0$. We find that in both the reset and the realistic models, for qubit-bath interaction parameters chosen from regions of the (x, y)-plane in Fig. 4.2 (reset model) and Fig. 4.7 (realistic model), the value of $\mathcal{W}$ is never positive during a typical evolution of the three-qubit state (see Fig. 4.8(f)). This indicates that no genuine tripartite entanglement is generated during the evolution, under both reset and realistic models of thermalization, when the qubit-bath interaction parameters are chosen according to CIP, such that transient refrigeration occurs without the steady-state refrigeration.

Note: We use two different sets of system parameters to carry out the study of quantum correlations for two different models of thermalization considered in this paper, and report the different behaviors of quantum correlations that are found in the chosen models. More specifically, in the case of the reset model, we choose $E_2 = 101, T_2 = 1, E_3 = 100, T_3 = 100$, while for the realistic model of thermalization, we choose $E_2 = 2, T_2 = 1, E_3 = 1, T_3 = 2$, with the latter values being chosen to avoid violations of the Markov approximation. Note here that if similar values of the system parameters were used for

both the models, then the behavior of quantum correlations would have been quite alike. For example, if we choose the energy and temperature values in the reset model to be the same as the harmonic oscillator bath model, no bipartite entanglement is generated during the dynamics.

4.3 Conclusion

In conclusion, we study the three-qubit self-contained quantum absorption refrigerator in such a parameter region of the system's dynamics where it is necessary to consider refrigeration in the transient regime. We propose a canonical form of the qubit-bath interaction parameters that facilitates the consideration of such a transient refrigeration without steady state cooling. With a modified canonical form of the qubit-bath interaction parameters, we show that a fast cooling of the cold qubit is also possible, where the coldest temperature is attained in steady state. Furthermore, we study the behavior of bipartite as well as multipartite quantum correlations in the three-qubit quantum refrigerator in a parameter space where transient cooling is the only option for refrigeration. We find that the system for which the thermalization process is modeled by heat baths consisting of an infinite number of oscillators, there appears a phenomenon of freezing of the minimum attainable temperature of the cold qubit with respect to change in system parameters. We believe that with the control on system-bath couplings, the necessarily transient cooling can be experimentally observed in the proposed realizations of quantum refrigerator. The qualitative features of the cooling phenomena as well as the behavior of quantum correlations in the two apparently different models of thermalizations are strikingly similar. However, the potential of this finding to be generic for any appropriate model of thermalization in the three-qubit quantum absorption refrigerator setup is a topic requiring further investigation. The cooling protocol can be generalized to more than three qubits, as long as the inter-qubit interaction is energy-conserving. However, more subsystems imply that, more control is needed in the set-up, which may turn out to be experimentally

challenging. Hence, from the point of view of resource optimization, a smaller dimension of the refrigerator is more desirable.

5

Adiabatic freezing of entanglement in t-J model

[1]As we have mentioned in the introduction of this thesis, there are situations when the environment-induced effects can be present in a system in such a way that it is complicated to derive a direct mathematical formulation of the interaction between the system and its environment. We will consider two different instances of such situations. In this chapter, we consider an instance where the environmental effect is manifested through an "effective" Hamiltonian of the system, and as an example of such cases, we will study a many-body system in presence of doping (with holes). To be specific, in this chapter we will study the entanglement dynamics in a one-dimensional t-J model. A different instance is considered in the succeeding chapter.

Over the years, a challenging task has been to explore how entanglement [7] is distributed among the constituents of a many-body system and understand its effects on cooperative phenomena [166–168]. For instance, it was observed that the constituents of the non-critical phases of many-body systems are, in general, less entangled with particles beyond their nearest neighbors (NN), and obey the area law of scaling of entanglement entropy [152, 169, 170], which provides useful information about their ground state properties [152, 166–168] and is closely related to its numerical simulability in canonical devices [171–175]. The study of quantum correlation, therefore, may actually provide a deeper insight about the underlying cooperative and critical phenomena in these sys-

[1]This chapter is based on Phys. Rev. B **98**, 125125 (2018)

tems [176–179]. In return, quantum many-body systems are also important substrates for quantum communication [180–182] and computation protocols [183–186], and are thus key enablers for quantum technology.

In this chapter, we report on the entanglement behavior in the ground state phases of a doped one-dimensional (1D) Hubbard model with large onsite interactions. The quantum spin-1/2 particles on the lattice doped with holes interact via the t-J Hamiltonian [187–189], with t representing a typical tunneling strength between two neighboring sites and J serving as the spin-spin interaction strength between particles in filled neighboring sites. The t-J Hamiltonian is widely used to study the physical properties of doped quantum spin systems, in particular for high-T_c superconducting phases of strongly-correlated matter [190–193]. The minimum energy configuration of the t-J Hamiltonian exhibits a rich phase diagram in the J/t-n_{el} plane, with n_{el} being the electron concentration or density, and has already been extensively studied using physical quantities such as ground state energy, spin correlation functions, and spin gap [194–199]. In this regard, one of our primary motivations is to investigate how quantum correlations, especially bipartite entanglement (BE) and multipartite entanglement (ME), behave in these different phases, and whether insertion of defects play a significant role in altering the entanglement properties.

The key finding of this work is the existence of entanglement in the ground state of the doped 1D t-J Hamiltonian, in particular at low electron densities, which remains invariant under perturbative changes to the J/t ratio, implying potential application in robust quantum technologies. The entanglement remains constant under perturbations of the system parameter, a phenomena reminiscent of the *adiabatic freezing* of quantum correlations [200] (cf. [14, 91, 201–205]), where the aforementioned quantities are completely insensitive or *frozen* with respect to changes in system parameters [200] or decoherence [201]. We observe that this adiabatic freezing behavior of entanglement is different for bipartite and multipartite cases, and is closely related to the relevant ground state phases of this model [194, 196–199]. To elaborate, we observe that at low J/t ratio

($J/t < 2$), for low n_{el}, when the system is known to lie in the metallic Luttinger liquid phase [196], two-site BE, as quantified by the logarithmic negativity [14, 28, 152, 206], decays polynomially with the increase in lattice distance, $r = |i - j|$, between the lattice sites i and j, which essentially signals the dominating long-range order in the phase. Interestingly, within the metallic phase, the BE is invariant to changes in the J/t ratio and is therefore adiabatically frozen. In contrast, at higher J/t ratio, superconducting spin-gap phase [197, 198] and electron-hole phase separation (PS) occurs [194], accompanied by an exponential decay of BE. Subsequently, the adiabatic freezing of BE is lost during the quantum phase transition. Of greater significance is the behavior of multipartite entanglement, which for low fixed values of n_{el}, remains adiabatically frozen for all values of the J/t parameter space. Using generalized geometric measure (GGM) [46] (cf. [43, 45, 207]) as the measure of genuine multipartite entanglement, we show that the variation of GGM across the J/t-n_{el} phase space, for low n_{el}, remains insignificant or nil under adiabatic changes of the J/t ratio. It is important to note that no such adiabatic freezing of ME is observed in the undoped anisotropic 1D model [208]. Rather counterintuitively, it appears that the presence of *impurities* or *defects* (as modeled by the holes) in the spin chain acts as a vehicle for phases with *frozen* ME. The importance of the results lie in the fact that many-body systems with robust ME, which is not sensitive to perturbations in system parameters or environmental processes, are necessary for realizing quantum information-theoretic protocols such as measurement based quantum computation [183] and quantum communication protocols [180, 182].

The chapter is arranged as follows. In Sec. 5.1 we introduce the 1D t-J Hamiltonian. We study the decay and adiabatic freezing of bipartite entanglement in Sec. 5.2. We demonstrate the freezing of genuine multipartite entanglement in Sec. 5.3, and we conclude in Sec. 5.4.

5.1 Model

In our study, we consider the t-J Hamiltonian as the structure that governs the interaction between the quantum particles in the doped 1D spin lattice, with N sites populated with $N_{el}(< N)$ quantum spin-1/2 particles. The rest of the sites are vacant or contain *holes*. The "electron density" of the lattice is given by n_{el} $(= N_{el}/N)$. The t-J Hamiltonian can be obtained perturbatively from the prominent Hubbard model in the limit of large on-site interaction [187], and has been expressed in literature in the form,

$$H = -t \sum_{\langle i,j\rangle,\sigma} \mathcal{P}_G \left(c^{\dagger}_{i\sigma} c_{j\sigma} + \text{h.c.}\right) \mathcal{P}_G + J \sum_{\langle i,j\rangle} \vec{S}_i \cdot \vec{S}_j, \tag{5.1}$$

where $c_{i\sigma}$ $(c^{\dagger}_{i\sigma})$ is the fermionic annihilation (creation) operator of spin σ $(= \{\uparrow, \downarrow\})$, acting on site i. $\mathcal{P}_G$ is the Gutzwiller projector $\Pi_i(1 - n_{i\uparrow} n_{i\downarrow})$ which enforces at most single occupancy at each lattice site. $S_i = \frac{1}{2}\sigma_i$'s are the triad of spin operators $\{S^x, S^y, S^z\}$, while t and J correspond to the transfer energy and the spin-exchange interaction energy terms, respectively, and each is limited to nearest-neighbor sites, with periodic boundary condition. The ground state phase diagram for the above 1D model has received widespread attention in the past years [194, 196–199]. In particular, the presence of three primary phases, namely the repulsive Luttinger liquid or metallic, attractive Luttinger liquid or superconducting, and the phase separation, have been predicted using exact diagonalization [196]. However, recent results, using density matrix renormalization group techniques, have also reported the presence of a superconducting spin-gap phase at low n_{el} [198, 199]. These phases play a significant role in the entanglement properties of the doped quantum spin model.

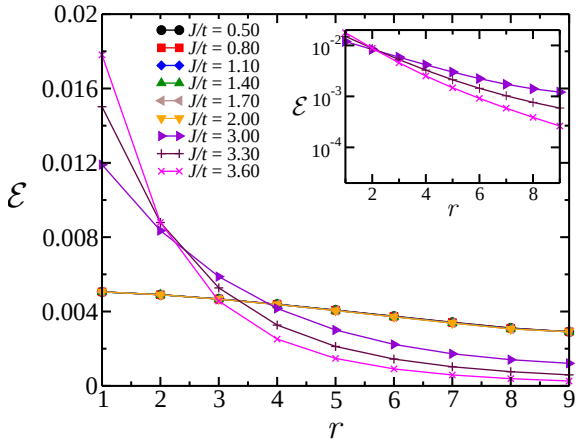

Figure 5.1: Decay and adiabatic freezing of bipartite entanglement in phases of the t-J Hamiltonian. The plot shows the variation of two-site entanglement ($\mathcal{E}$) with increase in lattice distance $r = |i - j|$, for the 1D t-J Hamiltonian, with $N = 30$ and $n_{el} = \frac{2}{N}$. For $J/t \leq 2$, the ground state remains in the metallic phase and $\mathcal{E}$ decays polynomially as $1/(A + Br)$, with r, exhibiting the presence of a dominating long-range order in the ground state. The values of $A = 162.6$ and $B = 18.9$, obtained from the average best-fitted curve, remains almost unchanged for all the curves in this phase, and BE is adiabatically frozen. This freezing behavior of bipartite entanglement is shown more clearly in Fig. 5.2. In contrast, for $J/t \geq 3$, the superconducting and PS phases leads to exponential decay of BE, given by $\mathcal{E} \sim C \exp(-\frac{r}{\xi})$, where ξ is the characteristic length and the constant C can be obtained from the best-fitted curve. ξ and C are dependent on J/t and the adiabatic freezing of BE is lost in this phase. The vertical axis are in ebits and the horizontal axes are dimensionless. J/t is also dimensionless. In the inset, we set the vertical axis in the logarithmic scale and plot $\mathcal{E}$ for $J/t \geq 3$.

5.2 Decay of bipartite entanglement and adiabatic freezing in metallic phase

We now focus on the behavior of bipartite entanglement in the ground state of the t-J Hamiltonian. In particular, we look at the logarithmic negativity ($\mathcal{E}$) in the state, ρ_{ij}, shared between two-sites i and j, and its decay with increase in lattice distance, $r = |i - j|$, for different phases of the model in the J/t-n_{el} plane. For a bipartite state ρ_{ij}, shared between two sites i and j, its logarithmic negativity is defined as

$$\mathcal{E}(\rho_{ij}) = \log_2(2\mathcal{N}(\rho_{ij}) + 1), \tag{5.2}$$

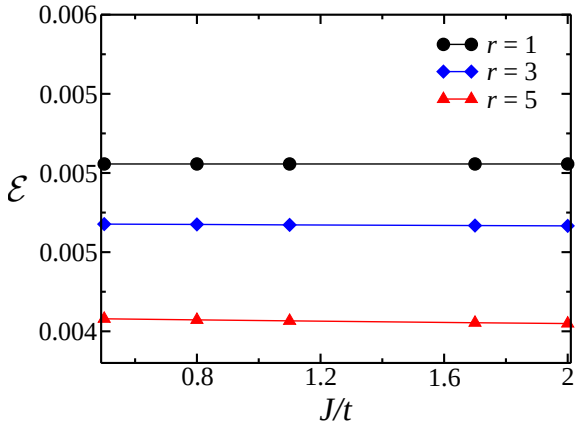

Figure 5.2: Adiabatic freezing of bipartite entanglement. Variation of two-site entanglement ($\mathcal{E}$) with J/t for different lattice distances, $r = |i - j|$=1 (black-circle), $r = 3$ (blue-diamond), $r = 5$ (red-triangle), for the 1D t-J Hamiltonian, with $N = 30$ and $n_{el} = \frac{2}{N}$. From the figure, one can see that for $J/t \leq 2$, the ground state BE remains adiabatically frozen. The vertical axis is in ebits and the horizontal axis is dimensionless. Although the region considered in the figure is $0.5 \leq J/t \leq 2$, the freezing behaviour extends all the way to $J/t = 0$.

where $\mathcal{N}$ is the negativity [14,206], defined as the absolute value of the sum of the negative eigenvalues of $\rho_{ij}^{T_i}$, so that $\mathcal{N}(\rho_{ij}) = \frac{\|\rho_{ij}^{T_i}\|_1 - 1}{2}$, where $\rho_{ij}^{T_i}$ denotes the partial transpose of ρ_{ij} with respect to the subsystem i.

The decay of spin correlation functions with inter-site distance r, often signals the nature of correlation present in the system [176, 177, 209]. In general, for non-critical states of strongly-correlated 1D spin systems, quantum correlations are short-ranged and decay exponentially with the increase of lattice distance [210], giving rise to features such as the area law [152, 169]. As discussed earlier, for all n_{el} in the J/t-n_{el} phase space, at low values of J/t (≈ 2), the ground state remains in a metallic phase or a repulsive Luttinger liquid-like phase [196]. In Fig. 6.2, we plot the decay of bipartite entanglement, $\mathcal{E}(\rho_{ij})$, with the lattice distance r, for different values of the J/t ratio, using exact diagonalization to obtain the ground state for $N = 30$ and $n_{el} = 2/N$. In the metallic phase ($J/t \leq 2.0$), the decay with respect to r can be encapsulated as $\mathcal{E} \sim 1/(Ar + B)$, where the numerically obtained values of A and B, from the best-fit curve, are given by $A = 162.6$ and $B = 18.9$, respectively. Significantly, the curves of $\mathcal{E}(\rho_{ij})$ with respect to r for different values of J/t

are almost invariant in the metallic phase, i.e., the decay is not only polynomial, but it is the same polynomial for all J/t (see Fig. 5.2 for a more clear illustration). The entanglement therefore remains adiabatically frozen under perturbations of J/t. It is known that in the Luttinger-liquid phase, the NN spin correlation functions are independent of J/t and the electron density [199]. Therefore, one can infer that the freezing of bipartite entanglement is characteristic of the ground state phase diagram of the 1D t-J model. However, for non-NN spin correlation functions there is a very slow variation with the system parameters. Therefore, the behavior of $\mathcal{E}$ in Fig. 6.2 not only expectedly follows the properties of spin correlation functions but also provides more insight about the ground state in the metallic phase. The freezing of bipartite entanglement with respect to system parameters can be advantageous for implementing quantum technologies that is robust to fluctuations in the system parameters, potentially due to errors in the preparation procedure [**?**].

In Fig. 6.2, for higher values of J/t (≥ 3), when the system subsequently enters into the superconducting and phase-separation region [196, 199], the ground state of the system is likely to be a spin liquid or superposition of the terms where all the spin-1/2 particles form clusters, leading to a distinctive electron-rich and hole-rich phase separation, respectively. Consequently, in these regions, spin correlation functions are likely to be short-ranged similar to undoped ground state of the Heisenberg model. In other words, for high J/t, an exponential decay of spin correlation functions is expected. From Fig. 6.2, it is quite prominent that as the J/t ratio increases, the BE measure $\mathcal{E}(\rho_{ij})$ exhibits an exponential decay with the increase of r, given by $\mathcal{E} \sim C\ \exp(-r/\xi)$, where ξ is the characteristic length of the decay. Again from the best-fit data, one can estimate the value of the constant C. As an example, for $J/t = 3.6$, the best-fitted plot yields $C = 0.0236$ and $\xi = 0.5225$. Interestingly, in contrast to the polynomial decay of BE in the metallic phase, the exponential decay rate is not constant for different values of J/t in the superconducting and PS phase. It is observed that the decay becomes steeper, with increase in J/t, such that entanglement vanishes quicker with r, and the freezing behavior is completely lost in these regions.

Moreover, if we introduce additional next-nearest neighbor interactions in the t-J Hamiltonian, the subsequent spin model is known to have a rich phase diagram in the J/t-n_{el} plane [197], which is qualitatively similar to that of the Hamiltonian in Eq. (5.1), apart from the fact that, in this case, the intermediate spin-gap phase is spread over a larger area in the phase plane. The boundaries between the metallic, superconducting, and PS phases are altered. Interestingly, the freezing of BE, or lack thereof, in the different phases remains unaltered.

5.3 freezing of multipartite entanglement

A significant outcome of our analysis of the entanglement properties of ground state phases of the 1D t-J Hamiltonian, is the existent characteristics of genuine multipartite entanglement. To measure the genuine ME in the different regions of the J/t-n_{el} plane, we use the generalized geometric measure (GGM) [46] (cf. [207]).

For an N-party pure quantum state $|\phi\rangle$, the GGM is a computable measure of genuine multisite entanglement, which is formally defined as the optimized fidelity-based distance of the state from the set of all states that are not genuinely multiparty entangled. Mathematically, the GGM can be evaluated as

$$\mathcal{G}(|\phi\rangle) = 1 - \lambda^2_{\max}(|\xi_N\rangle),$$

where $\lambda_{\max} = \max |\langle\xi_N|\phi\rangle|$, and $|\xi_N\rangle$ is an N-party non-genuinely multisite entangled quantum state and the maximization is performed over the set of all such states. The GGM can be effectively computed using the relation

$$\mathcal{G}(|\phi\rangle) = 1 - \max\{\lambda^2_{A:B} | A \cup B = A_1, \ldots, A_N, A \cap B = \phi\},$$

where $\lambda_{A:B}$ is the maximum Schmidt coefficient in all possible bipartite splits $A : B$ of

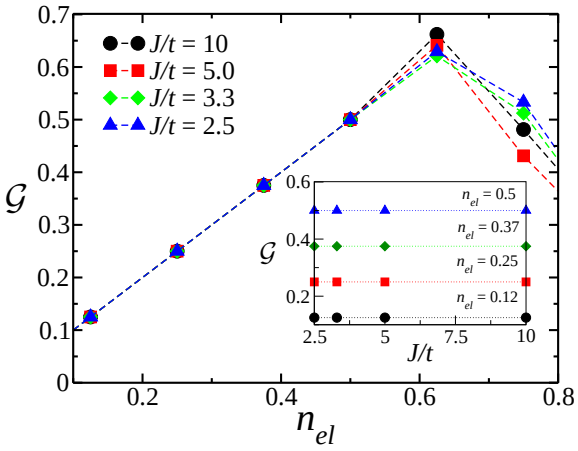

Figure 5.3: Adiabatic freezing of genuine multipartite entanglement. The plot shows the variation of the generalized geometric measure, $\mathcal{G}$, with n_{el} for different values of J/t. The number of lattice sites in the 1D model is fixed at $N = 16$. At low electron density, viz. $n_{el} \lesssim 0.5$, $\mathcal{G}$ increases linearly, *along the same line*, with n_{el}, and reaches its maximum value at $n_{el} \approx 0.6$. This feature remains invariant for any value of the J/t ratio. However at large n_{el}, $\mathcal{G}$ becomes a function of system parameters and the feature – of increasing along the same line – obtained earlier, disappears. The inset shows that $\mathcal{G}$ is frozen with respect to change in J/t, for low n_{el}. The axes dimensions are the same as in Fig. 6.2.

the given state $|\phi\rangle$. A complexity in computation of the multiparty entanglement measure $\mathcal{G}$ lies in the fact that the number of possible bipartitions increases exponentially with an increase of the lattice size. Therefore, we need to restrict ourselves to moderate-sized systems only, which in our case restricts us to $N = 16$. We observe that at low electron concentrations the GGM is adiabatically frozen over significant regions of the phase space.

We study the variation of GGM in the ground state of the 1D t-J Hamiltonian, with respect to system parameters J/t and n_{el}, as depicted in Fig. 5.3. For convenience in representation, we look at higher values of J/t (≥ 2.5), corresponding to the superconducting and PS phases of the model. We observe that $\mathcal{G}$ increases linearly with n_{el}, at low values of n_{el}, for fixed J/t. It reaches a maximum at $n_{el} \approx 0.6$, thereafter decreasing with further increase in n_{el}. This behavior is similar to the ground state properties of spin liquid phases in doped Heisenberg ladders [211]. Significantly, in the low electron density regime, i.e., $n_{el} \lesssim 0.5$, the genuine multisite entanglement ($\mathcal{G}$) is insensitive to the parameter J/t, and is thus adiabatically frozen. We have numerically observed that at low n_{el} this phenomenon

extends to lower values of J/t. However, this freezing of GGM completely vanishes as the electron density is increased. We note that such adiabatic freezing of ME is not observed in other models, for instance in the undoped anisotropic 1D model [208].

This highlights a set of very unique features of the ground state phases of the 1D t-J Hamiltonian. In particular, in the metallic Luttinger liquid phase, at low J/t and n_{el}, bipartite entanglement is long-ranged and adiabatically frozen, in stark contrast to the exponentially decaying BE in superconducting and PS phases. However, at low n_{el} but all J/t, including the latter phases, multipartite entanglement is frozen and completely invariant to system parameters. This provides an interesting interplay between the behavior of BE and ME in different phases of the doped Hubbard model.

5.4 Conclusion

Entanglement is an important resource in quantum information protocols [7, 166, 167]. However, in general, both bipartite and multipartite entanglement are fragile to decoherence [212–215], and this is one of the main obstacles in realization of these protocols. The entanglement may also be highly sensitive to perturbative or sudden changes in system parameters and may fluctuate close to critical points, as observed during collapse and revival [216, 217] and dynamical transitions of entanglement [218]. Certain information-theoretic quantum correlations, such as quantum discord, could exhibit freezing in the face of decoherence [203], espousing a strong belief that this could lead to robust information protocols. However, entanglement, the workhorse of key quantum information protocols, rarely freezes under system parameter or temporal changes, including under decoherence (cf. [219, 220]). Our results show that doped quantum spin chains described by the 1D t-J Hamiltonian contain ground state phases that exhibit adiabatic freezing of both bipartite and genuine multisite entanglement. Interestingly, the same model without the insertion of defects – in the form of doping – does not exhibit a similar freezing

phenomenon [208]. It is the presence of defects in the quantum spin system that gives rise to the nascent phenomenon of adiabatic freezing of entanglement. The bipartite and multipartite entanglement in such systems can potentially be used as a resource in quantum protocols. An important observation in this regard is that no freezing phenomenon of multiparty entanglement (or other multiparty quantum correlations) has hitherto been observed in any quantum system. For applications in other quantum information protocols, such as fault-tolerant [186] or one-way computation [183], robustness of multisite entanglement over fluctuating system parameters can be a significant resource in achieving desired levels of stability.

6

Inhibition of spreading in quantum random walk

[1]In this chapter, we will discuss the effects of disorder, due to a noisy environment, in the system parameters of a one-dimensional quantum random walk (QRW). The classical counterpart of QRW - the classical random walks (CRWs) - have already been established as useful tools in classical randomized algorithms [221]. The Markov chain model of CRW has succeeded in estimating the volume of a convex body [222] and Markov chain Monte Carlo simulation has been able to approximate the permanent of a matrix [223]. Random walk in a quantum mechanical scenario was introduced in 1993 by Aharonov *et al.* [224]. Since their work, QRWs have been studied extensively, using both the discrete time [225, 226] as well as continuous time [227, 228] models.

An important feature of a QRW that makes it so different from a CRW is the faster propagation of the wave function compared to a classical walker. This happens due to the interference between different possible paths that the wave function can propagate in. For a CRW on a line, the standard deviation goes as the square root of the number of iterations, whereas for QRWs on a line, the distribution spreads linearly (ballistic propagation) with increasing number of iterations [229]. This trait of QRWs has been extremely helpful in developing numerous quantum algorithms, e.g. in investigating the exponentially faster hitting time of QRW over CRW [228, 230, 231], and in various quantum search algorithms [232, 233]. On the other hand, in the field of condensed matter,

[1]This chapter is based on Phys. Rev. A **99**, 042329 (2019)

there has been investigations to realize topological phases that are not possible to be described by local order parameters, in controlled systems composed of photons [234] or cold gases in optical lattices [235, 236]. In [237], it has been shown that discrete time QRWs permit the experimental study of the whole class of topological phases in one and two dimensions [238, 239].

One-dimensional QRWs have been experimentally realized in a number of physical systems e.g. in trapped ions [240, 241], nuclear magnetic resonance systems [242–244], photons in waveguides [245–247], to mention a few. QRWs have also been applied in simulation of physical processes like photosynthesis [248, 249], quantum diffusion, and breakdown of electric-field driven systems [250, 251]. See Refs. [252–258] for further applications.

However, this ballistic propagation of the wave function is significantly inhibited when randomness is introduced in the substrate or medium [257, 259, 260]. More precisely, an inhomogeneity in the medium breaks the periodicity of the medium and hence gives rise to suppression of spread of the wave function at certain regions/points of the lattice which remains unchanged with time. This is similar to the localization phenomena in condensed matter physics, first studied by Anderson [261] in the context of electron localization in a disordered lattice. Another way of obtaining such reduction in spread in QRWs is by introducing disorder in the operations that control the dynamics of the system instead of directly making the medium inhomogeneous. This kind of inhibition of spread in discrete-time QRWs is observed by inducing disorder in the coin rotation at each iteration or by introducing phase-defects at selective sites. In the first case, during each coin flip, the rotation angle of the coin is randomly selected from some probability distribution [262, 263]. In the second case, the quantum walker picks up a particular phase factor whenever it passes through some particular site or sites [191, 264]. The motivation behind studying QRW in presence of disorders lies in the fact that in real systems, it is hardly possible to completely get rid of all kinds of inhomogeneity or noise. For example, the

external radiation controlling the motion of an atom in an array of optical lattices, can have a time-dependent disorder, or the distance between two adjacent optical lattices can vary. It is important to investigate the localizing effect of the disorder, as the same can have implications for speed-up effects in search algorithms and other applications of the nonclassical speed in the propagation of the quantum walker.

In this chapter, we focus on discrete-time QRWs with a different type of channel of disorder. We introduce a quenched Poisson-distributed randomness in the length of the jump that the quantum walker takes after each coin toss, and study the resultant probability distribution on the position space after a large number of iterations. Poisson distributions with different means are considered. We observe that the walker is constrained to remain near its initial position, with the quenched averaged spread being in a regime that is sub-ballistic but super-diffusive. The qualitative behavior of inhibition of spread is independent of the mean. We also find that the feature remains qualitatively unaltered in systems where the jumps have certain sub- and super-Poissonian distributions. We have also studied the differences in the response on the quenched averaged spread by changing the disorder from dynamic to static. Disorder in the jump of the walker can potentially be realized in systems where QRWs have been studied experimentally. For example, in the QRW of a single laser-cooled Cs atom on a one-dimensional optical lattice [265], errors in the voltage that controls the movement of the atom from one lattice site to another during the shift operation can be modelled by a QRW with a disorder in its jump. A similar possibility exists for QRWs executed using $^{25}Mg^{+}$ ions on a lattice [241]. See also [266].

The chapter is organized as follows. In the next section, we give a short introduction to discrete-time quantum walks on a line. In Section 6.2, we briefly describe the concept of quenched disorder and the corresponding quenched averaging, while in Section 6.3, we formally define the Poisson distribution. In Section 6.4, we present our results on the effect on a QRW of a Poisson-distributed quenched random variable being used as the length of the jump of the quantum random walker. In Section 6.5, we consider the case

when the Poisson distribution is replaced by certain sub- and super-Poissonian distributions. Section 6.6 considers the case of static quenched disorder. We present a summary in Section 6.7.

6.1 Discrete-time quantum walk

In analogy to CRWs, the displacement of the particle on the one-dimensional lattice in discrete-time quantum walk is associated with the tossing of a "quantum coin". Suppose that $\mathcal{H}_p$ denotes the Hilbert space corresponding to the position of the particle. For a one-dimensional walk of T "iterations", a basis of $\mathcal{H}_p$ is $\{|i\rangle : i \in [-T, T] \cap \mathcal{Z}\}$, with $\mathcal{Z}$ being the set of all integers. The Hilbert space, $\mathcal{H}_c$, of the coin is spanned by two basis states, say, $|0\rangle, |1\rangle$. But unlike CRWs, the state of the quantum coin can be in superposition of the two basis states. The particle executing the quantum random walk moves one step towards right if the coin state is $|0\rangle$ and towards left if the coin state is $|1\rangle$, but unlike CRWs, the process happens coherently, much like the quantum parallelism in quantum computer circuits [78]. This conditional shift operation is described by the operator

$$\tilde{S} = \sum_{i=-T+1}^{T-1} (|0\rangle\langle 0| \otimes |i+1\rangle\langle i| + |1\rangle\langle 1| \otimes |i-1\rangle\langle i|)\,. \tag{6.1}$$

The random walk procedure begins with a rotation in the coin space, which is analogous to the tossing of a coin in CRW. The coin rotation can be any unitary operation on the coin Hilbert space, thus generating a rich family of random walks. Here we consider the Hadamard coin for which the initial rotation is the Hadamard gate, given by

$$H = \frac{1}{\sqrt{2}} \begin{pmatrix} 1 & 1 \\ 1 & -1 \end{pmatrix}, \tag{6.2}$$

Suppose also that initially the particle is at the origin, for which the particle state is $|0\rangle$, and that the initial state of the coin is $|0\rangle$. In each iteration of a given run of the experiment,

we apply the Hadamard rotation on the coin and then apply the shift operation on the joint system of the coin and the particle. So, after the first iteration, the joint state of the coin-particle system can be represented as

$$\begin{aligned}\tilde{S}\,(H \otimes \mathbb{I})|0\rangle \otimes 0\rangle &= \tilde{S}\,\frac{1}{\sqrt{2}}(|0\rangle + |1\rangle) \otimes |0\rangle \\ &= \frac{1}{\sqrt{2}}(|0\rangle \otimes |1\rangle + |1\rangle \otimes |-1\rangle),\end{aligned} \tag{6.3}$$

where $\mathbb{I}$ denotes the identity operator on $\mathcal{H}_p$. We iterate this process T times without performing any measurement at the intermediate iteration times. Therefore, after T iterations, the state of the coin-particle duo reads $[\tilde{S}\,(H \otimes \mathbb{I})]^T|0\rangle \otimes |0\rangle$. For a CRW, in the limit of a large number of iterations, the position of the particle is Gaussian distributed, with the standard deviation diverging only as $\sqrt{T}$. On the other hand, the state $[\tilde{S}\,(H \otimes \mathbb{I})]^T|0\rangle|0\rangle$ has a standard deviation that diverges as T. Note that in the limit $T \to \infty$, the scaling of standard deviation of the probability distribution of the walker with respect to number of steps taken, was analytically derived in [267–269].

6.2 Quenched disorder

In this work, we consider a category of disorder, which, to our knowledge, has not yet been studied for quantum random walks. In a QRW, at every iteration, the walker is displaced by one step, conditioned on the coin state. There is, therefore, an already existing randomness in quantum walks due to the superposition between the two coin states that is created at each iteration by the Hadamard gate. Let us introduce an additional randomness in the amount of displacement of the particle at each time step. In [260], Lavička *et al.* introduced a randomness in the jump length for quantum random walk in optical multiports, where they considered that the quantum walker, at each coin toss, can jump to the next multi-port with some probability δ, or can connect to a multiport at a fixed distance with probabilty $(1 - \delta)$. Unlike Lavička *et al.* and unlike in the case without disorder, in

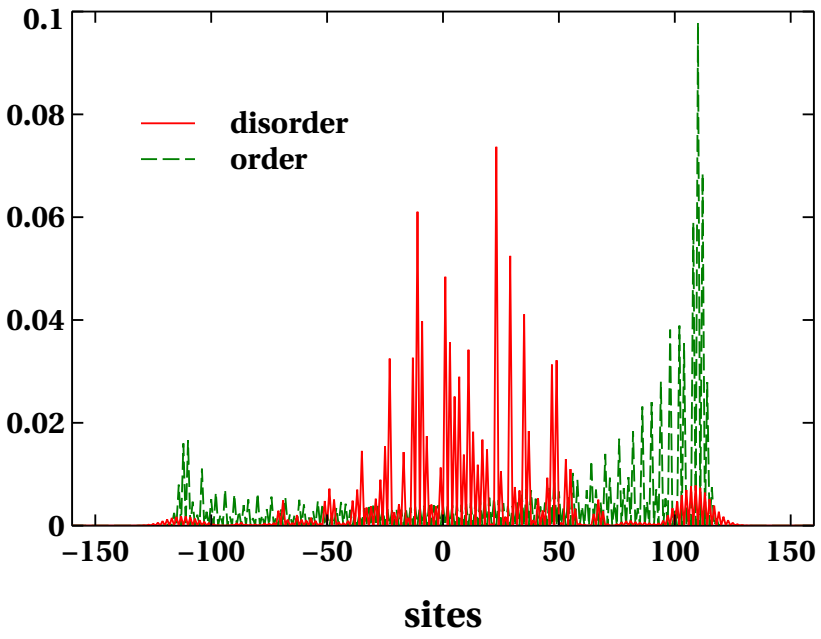

Figure 6.1: Comparison of the ordered quantum walker with a disordered one. We compare the site probabilities of a quantum random walker without disorder (green, dashed) with the same for one with Poisson-distributed disordered step-size (red, solid), for 160 iterations. The vertical axis represents the site probabilities after 160 iterations, while the horizontal axis represents the sites, with the origin of the horizontal axis representing the initial position of the walker. The probabilities for the disordered case are for a particular realization of the disorder. A comparison of the site probabilities for the disordered walk, with those of the ordered case clearly indicates that disorder causes the quantum walker to remain in the near-origin region, albeit only for the particular realization of the disorder. The same feature is seen for other realizations of the disorder, and we will see in subsequent analysis that a quenched averaging over a large number of disorder realizations provides a clearer signature of what is akin to "localization", and which is referred to in this chapetr as "inhibition of spread". Both axes represent dimensionless quantities.

our case, after each coin toss, the walker can jump an arbitrary number of steps with the length, j, of the jump being randomly distributed according to a certain discrete probability distribution $\mathcal{P}_{\mathcal{R}}(j)$, where $\mathcal{R}$ denotes the effective maximal jump. This jump length j is the same irrespective of which vertex the particle is in at that time-step. Moreover, the jump length is also the same, albeit in different directions, regardless of whether the quantum coin is "thrown" into the $|0\rangle$ or the $|1\rangle$ state by the Hadamard operator of that iteration. Note that, when $j = 0$, the walker stays at its current position. Introduction of this kind of disorder can be described by the shift operator given by

$$\tilde{S}' = \sum_{i=-(T-1)\mathcal{R}}^{(T-1)\mathcal{R}} \left(|0\rangle\langle 0| \otimes |i+j\rangle\langle i| + |1\rangle\langle 1| \otimes |i-j\rangle\langle i|\right), \tag{6.4}$$

where j takes values from $\{0, 1, \ldots, \mathcal{R}\}$ according to the distribution $\mathcal{P}_{\mathcal{R}}(j)$, and the coin operation is taken to be Hadamard. Values of j higher than $\mathcal{R}$ are either non-existent or are ignored for some physical reason (e.g. insignificant effect on the position probabilities for allowing $j > \mathcal{R}$). Note that the Hilbert space of the walker has now changed into one that is spanned by $\{|i\rangle : i \in [-T\mathcal{R}, T\mathcal{R}] \cap \mathcal{Z}\}$.

The disorder that is introduced in the step length at every iteration of the protocol is "quenched", so that it remains fixed for the entire span of a particular run of the protocol. To obtain a meaningful value of a physical quantity, say, the dispersion of a walker in a quenched disordered system, one must perform a configurational averaging over the disordered parameters. Note that this averaging needs to be performed only after all other calculations have already been performed. Such an averaging is referred to as "quenched averaging". We are in particular interested in quenched averaged dispersion of QRWs, in which the step length at different iterations of the protocol are independent and identically distributed quenched random variables distributed as $\mathcal{P}_{\mathcal{R}}(\cdot)$.

6.3 Poisson distribution

The Poisson distribution, due to A. de Moivre and S. D. Poisson, is a discrete probability distribution which gives the probability of the number of occurences of a certain event in a fixed interval, as

$$p(k) = \frac{e^{-\lambda}\lambda^k}{k!}, \tag{6.5}$$

where λ is the average number of events that occur in the given interval and $p(k)$ is the probability that the event will occur k times in that interval. The Poisson distribution is known to be useful in a large variety of situations. Examples include the number of mails received per day by a particular office, the number of scientific papers published in a month from a certain institute, the number of trains canceled in a week on a particular route, etc. In this work, we begin by using the Poisson distribution around the average $\lambda = 1$ to randomly generate the integer values of j (see Eq. (6.4)). For numerical convenience, we have discarded all those random outcomes where $j > 5$, and have renormalized the resulting distribution. Note that for $\lambda = 1$, the probability that $j > 5$ is of the order of 10^{-4}.

6.4 Inhibition of spread

Let us first briefly examine the results for the discrete quantum walk with no disorder in the system. We assume the coin to be initially in the state $|0\rangle$ and the particle to be initially at the origin. We apply the Hadamard gate on the coin, following which the shift operator as in Eq. (6.1) is applied on the particle. This process is repeated several times, and the probability distribution of the walker's position after 160 iterations is depicted in Fig. 6.1. We find that the walker has a high probability to be around $i = 100$ after 160 iterations. We are mainly interested in studying the standard deviation of the probability distribution in the particle space. In this case, as expected, the standard deviation, σ,

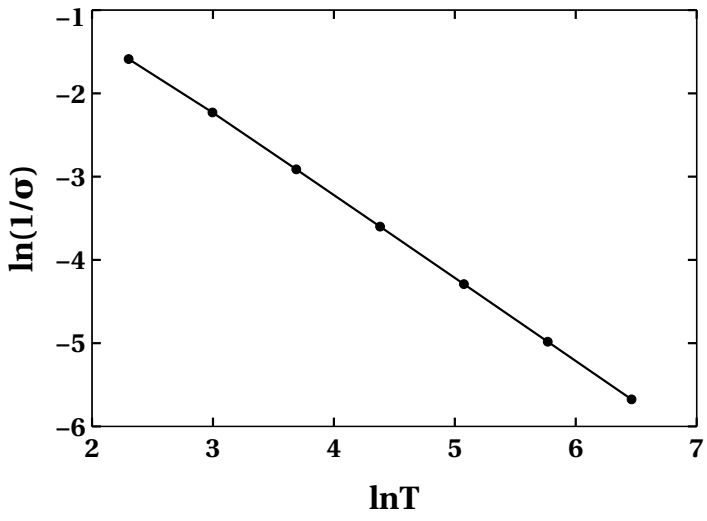

Figure 6.2: Scaling behavior of the dispersion in the ordered qauntum random walk. We plot $\ln(1/\sigma)$ against $\ln T$ for up to 640 iterations to find a straight-line fit, and with a slope of -1. All quantities are dimensionless. See [267–269].

varies linearly with the number of iterations, T. We perform a log-log scaling analysis between $\ln(1/\sigma)$ and $\ln T$ (see Fig. 6.2) to find a straight-line fit. The slope of the straight line is $\tan(-\pi/4) = -1$. A QRW with a σ that is linearly varying with respect to the number of iterations is usually referred to as "ballistic propagation" of the particle.

QRWs appears in several colors and hues, encompassing discrete as well as continuous walks. Disorder in such systems have also been incorporated in different ways. This includes e.g. [259], which incorporates an imperfection in the graph which supports a continuous-time walker, resulting in an inhibition of spread of the latter on the graph at the starting point. Another work [257] associates a transgression in the dynamical equation of the continuous-time quantum random walker, wherein there can appear situations where the walker remains virtually unmoved. The corresponding reduction in spread depends on the type of disorder involved, and the consequences can also vary from being "diffusive" (standard deviation of the walker is proportional to the square root of the number of iterations) to being ballistic. A discrete-time QRW with non-Hadamard operations at each toss of the quantum coin was considered in [262]. The non-Hadamard operator was chosen to be different at each iteration, and the result was a suppression of

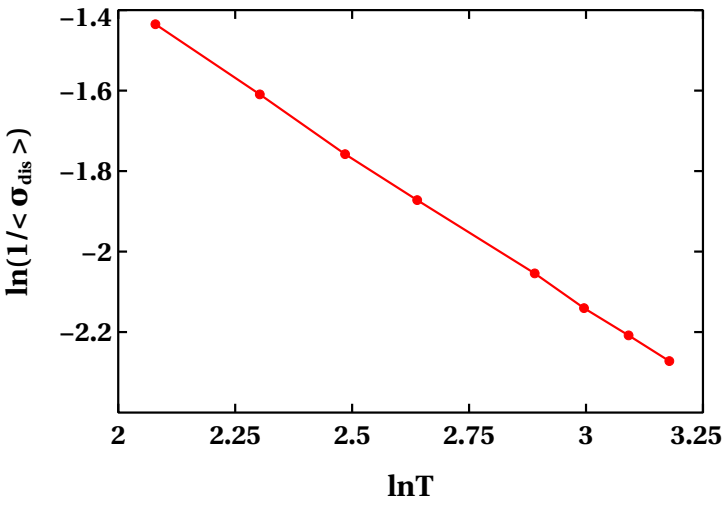

Figure 6.3: Scaling behavior of dispersion in the quenched-disordered quantum random walk. We plot $\ln(1/\langle\sigma_{dis}\rangle)$ against $\ln T$ for up to 24 iterations to find a straight-line fit, just as in Fig. 6.2. However, the slope in the disordered case is given by $\tan\theta \approx -0.8$. All quantities are dimensionless.

the wave function of the walker to its initial point. Further such cases can be found e.g. in [270, 271]. In another example, Ref. [191] finds that a non-Hadamard quantum coin associated with a discrete-time quantum walker can confine or repulse the walker at or from its initial point depending on the phase of the rotation in the quantum coin at each iteration. See also [263, 264] in this regard.

In this work, we consider the quantum random walk, where we have included a disorder in the number of steps, j, the particle can go after each tossing of the coin. We begin by examining the case where j is randomly chosen from the Poisson distribution with unit mean. Here we first apply the Hadamard gate on the coin, following which the shift operator as in Eq. (6.4), is applied on the particle. After T iterations, we calculate the standard deviation σ_{dis}, for the particular realization of the disordered variables. In Fig. 6.1, we provide a comparison between the probabilties in the cases when there is no disorder, and when there is a particular realization of the Poisson-distributed disorder. It is clear from the figure that the disorder hinders the walker's movement to regions away from its initial position, albeit only for the particular realization of the disorder considered in Fig. 6.1 (cf. [257, 259]). We will see that the inhibition in spread observed here

persists even after a quenched averaging. The jump or shift, j, at any iteration of a particular run is considered to be independent from but identically distributed with the jump in any other iteration of that run. The physically relevant quantity, however, is the average of this σ_{dis} for different realizations of the disorderd variables. We denote this quenched avaraged σ_{dis} as $\langle\sigma_{dis}\rangle$. Our numerical simulations show that with increasing number of iterations, T, $\langle\sigma_{dis}\rangle$ diverges to infinity, just like in case of the ordered system, but the divergence is much slower. The quenched averaging is performed over 4000 disorder realizations. Here, the "finite-size" scaling exponent is ≈ 0.8, as compared to unity in the case of the ordered system. The "finite-size" here refers to the finite number of iterations, and corresponds to the finite number of subsystems in finite-size scaling analysis in many-body physics. The finite-size analysis can be stated more precisely by expressing the disorder-averaged dispersion as

$$\ln\left(\frac{1}{\langle\sigma_{dis}\rangle}\right) = -\alpha \ln T + \ln A, \tag{6.6}$$

so that

$$\langle\sigma_{dis}\rangle = A^{-1} T^{\alpha}, \tag{6.7}$$

where $A \approx 1$ and $\alpha \approx 0.8$, up to the first significant figure. See Fig. 6.3, and compare with Fig. 6.2. The disorder, therefore, induces a standard deviation of the walker that is intermediate to being ballistic and diffusive. It is sub-ballistic but super-diffusive.

We also try to look at the effects of changing the mean of the Poisson distribution to values other than unity. The results have been summarized in Table 6.1. We observe that for different means, the value of the scaling exponent is in the range -0.8 to -0.7.

Below we find that this behavior of having an intermediate scaling exponent (sub-ballistic but super-diffusive) of standard deviation is far more general, and can be seen in types of disorder, widely varying from the Poissonian one.

Distribution	**Mean**	**Scaling exponent**
Poisson	0.5	-0.8
	1.0	-0.8
	1.5	-0.7
	2	-0.7

Table 6.1: Sub-ballistic but super-diffusive spread for quenched Poisson disorder with different values of the mean. The tabular data presents the scaling exponent α when the jump length of the quantum walker is chosen from Poisson distributions having different mean values.

Class	**Distribution**	**Variance**	**Scaling exponent**
	Poisson	1	-0.8
Sub-Poissonian	Binomial	1/2	-0.8
		8/9	-0.8
	Hypergeometric	1/3	-0.8
Super-Poissonian	Negative binomial	2	-0.8
		10/9	-0.7
	Geometric	2	-0.8

Table 6.2: Sub-ballistic but super-diffusive spread for different classes of quenched disordered discrete distributions of the jump length in a quantum random walk. We present here the values of the scaling exponent α obtained in cases when the jump length is randomly chosen from Poisson and certain paradigmatic sub- and super-Poissonian distributions. The corresponding variances are also indicated in the table. All the distributions have unit mean.

6.5 Sub- and Super-Poissonian distributions

From the Poisson distribution, let us now move over to one-dimensional QRWs where j is randomly chosen according to certain paradigmatic sub- and super-Poissonian distributions. A sub- (super-) Poissonian distribution has a smaller (larger) variance than the Poisson distribution having the same mean. As examples of sub-Poissonian distributions, we consider the binomial and hypergeometric distributions, while as examples of super-Poissonaian distributions, we perform our analysis by considering the negative binomial and geometric distributions.

The *binomial distribution* is a discrete probability distribution involving Bernoulli trials, with the latter being independent and identically distributed (i.i.d.) trials that have two outcomes, called "success" and "failure". The total number of trials is fixed to a certain integer n, and the random variable is the number of successes, k, occuring at each trial with probability p. The probability mass function (pmf) is given by $\binom{n}{k}p^k(1-p)^{n-k}$, with the mean and variance being np and $np(1-p)$ respectively. Note that the variance is lower or equal to the mean.

The *hypergeometric distribution* is a discrete probability distribution where one is given a finite population having size N within which there are exactly K elements that we refer to as "successes". The random variable is the number k of successes in a particular trial of n draws without replacement. The pmf of the hypergeometric distribution is therefore given by $\frac{\binom{K}{k}\binom{N-K}{n-k}}{\binom{N}{n}}$. Unlike the binomial distribution, here, after each draw, the probability of success changes. The mean and variance of this distribution is given by $\frac{nK}{N}$ and $\frac{nK}{N}\frac{N-K}{N}\frac{N-n}{N-1}$, so it has a varinace lower than the mean, i.e. it is a sub-Poissonian distribution.

The *negative binomial distribution* is also a discrete probability distribution involving Bernoulli trials. The random variable in this case is the number of successes, k, until a specified number, r, of failures, with the fixed probability of success in each trial being p.

The corresponding pmf is given by $\binom{k+r-1}{n}(1-p)^r p^k$. The mean of the negative binomial distribution is $\frac{pr}{1-p}$, while the variance is $\frac{pr}{(1-p)^2}$. Note that the variance is then always larger or equal to the mean.

The *geometric distribution* is a discrete probability distribution involving Bernoulli trials. Here, the random variable is the number, k, of failures before the first success occurs, with probability of success in each trial being p, so that the pmf is given by $p(1-p)^k$. The mean and variance are given by $\frac{1-p}{p}$ and $\frac{1-p}{p^2}$, so that the distribution has a variance greater than the mean, i.e. it is a super-Poissonian distribution.

For demonstration, we choose two (sub-Poissonian) binomial distributions having two different variances, respectively $\frac{1}{2}$ and $\frac{8}{9}$, and one (sub-Poissonian) hypergeometric distribution with variance $\frac{1}{3}$; note that the variances are *smaller* than their common unit mean. Parallely, we choose two (super-Poissonian) negative binomial distributions having two different variances, respectively 2 and $\frac{10}{9}$, and one (super-Poissonian) geometric distribution with variance 2; note that the variances are *larger* than their common unit mean. For each of the six cases, we perform the scaling analysis by plotting $\ln(1/\langle\sigma_{dis}\rangle)$ against $\ln T$. Interestingly, in all the cases, the scaling exponent reduces compared to the unit value in the ordered walk. The scaling exponents remain in the range -0.8 to -0.7. The set of data thus obtained is summarized in Table 6.2. In all the cases, the disorder averagings are performed over 4000 realizations, and the effective maximal jump ($\mathcal{R}$) is chosen so that the total probability to jump further is of the order 10^{-4} or less.

6.6 Effect of static disorder

The disorder considered in this work till now is dynamic in nature, i.e. the random jump length is different for different time-steps. We now study the effect of introducing a static quenched disorder in the jump length. In this case, associated to each site, there is a particular integer, fixed for all time, but random with respect to sites. The quantum walker,

after reaching a particular site, will take the next jump having a jump length equal to the integer associated to that site. We choose the integers randomly from a Poisson distribution with unit mean, and calculate the standard deviation of the probability distribution after a certain number of steps. Then we take a large number of such random integer configurations, to find the quenched averaged standard deviation. We find that the quenched averaged standard deviation grows almost linerarly with T for a relatively small number of steps, T, but for $T > 10$, it saturates to a value $\langle\sigma_{dis}\rangle|_{T\gtrsim 10} \approx 1.8$.

6.7 Conclusion

We introduced a quenched disorder in the number of steps that the quantum particle (walker) can jump after each coin toss in a discrete quantum random walk in one dimension. We found that the spread of the walker, as quantified by its standard deviation, after quenched averaging over a large number of configurations of the disorder, has a finite-size scaling exponent which is approximately 20% lower than that for the ordered case, thereby implying a slowdown of the walker. The speed of the walker is consequently sub-ballistic but super-diffusive. We then argued that this feature of the scaling exponent is generic, as it was found to be shared by random distributions widely varying from the Poissonian one. Inhibition of spread of the quantum random walker was also found for static quenched disorder. The effects studied can potentially be observed with currently available technology in systems where quantum random walks have been experimentally realized, in particular with atoms hopping on an optical lattice.

Keywords for thesis of Sreetama Das

Enrolment no.: PHYS08201305005

1) Open quantum system
2) Non-Markovian dynamics
3) Quantum thermodynamics
4) Quantum refrigerator
5) Quantum entanglement
6) Many-body system entanglement
7) t-J model
8) Freezing of entanglement
9) Quantum random walk
10) Disordered quantum random walk

Thesis Highlight

Name of the Student: Sreetama Das **Enrolment No.:PHYS08201305005**
Name of the CI/OCC: Harish-Chandra Research Institute, Prayagraj
Thesis Title: Quantum information processing in noisy environments
Discipline: Physical Sciences **Sub-Area of Discipline: Quantum Information**
Date of viva voce: 18th December, 2020

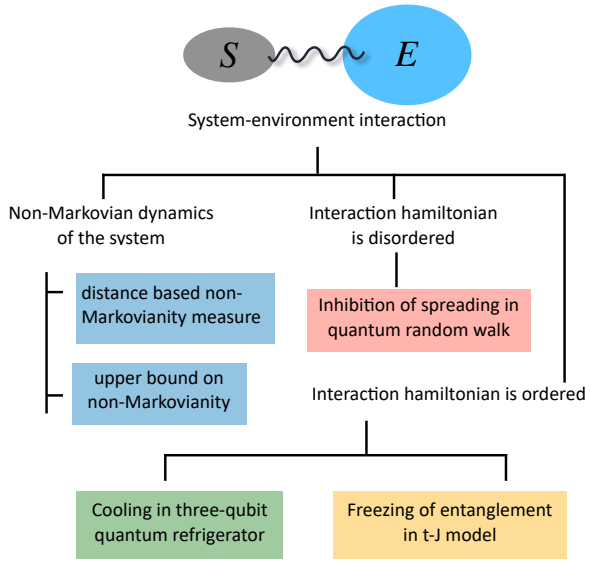

In this thesis, I study various aspects of quantum information processing in open quantum systems, in presence of environmental noise and disorder. I propose a new distance-based measure of non-Markovianity. A set of dynamical maps are constructed, which is called "ϵ-Markovian" maps of an open quantum system. I then define the "ϵ-nonmarkovianity" of any general dynamical map as the minimized distance of this map from the set of ϵ-Markovian maps. I also analytically derive an upper bound on the ϵ-nonmarkovianity. In the special case $\epsilon = 0$, this bound depends on the entanglement between system and environment.

I study a number of physical systems where the effect of interaction with environment is prominent. The first one is a three-qubit quantum refrigerator, where each qubit is in thermal contact with respective thermal baths. The qubits are interacting among themselves as well as with the thermal baths. I show that there exists a region in the qubit-bath interaction parameter space, where it is possible to obtain significant cooling of one of the qubits in the transient regime of the refrigerator, whereas the steady state cooling is negligible. In the second example, I show that in a fermionic system described by *t-J* model, the bipartite entanglement remains frozen with respect to adiabatically changing system parameters in the metallic phase. In contrast, the multipartite entanglement is frozen across all phases. This is of supreme importance in quantum information protocols where entanglement is a useful resource.

In the third example, I consider a disordered one-dimensional quantum random walk. After each coin toss, instead of taking one step left or right, the walker can jump arbitrary number of steps. This number is randomly chosen from Poissonian and certain sub- and super-Poissonian distributions. The scaling of the quenched-averaged standard deviation with time steps gives a scaling exponent around 0.7, which is less than the ordered quantum walk that have scaling exponent 1. This implies that the disorder has lead to an inhibition to the spreading of the quantum walker.

From the above observations, I conclude that- whereas the environmental effect can be detrimental, such as reducing the speed of a quantum walker, it can also be useful in certain scenarios, such as obtaining cooling in a system of interacting qubits and baths, and freezing the entanglement with respect to fluctuating system parameters.